

# Improved TMD factorization for forward dijet production in dilute-dense hadronic collisions

P. Kotko<sup>1</sup>, K. Kutak<sup>2</sup>, C. Marquet<sup>3</sup>, E. Petreska<sup>3,4</sup>, S. Sapeta<sup>5</sup> and A. van Hameren<sup>2</sup>

<sup>1</sup> *Department of Physics, Penn State University  
University Park, 16803 PA, USA*

<sup>2</sup> *The H. Niewodniczański Institute of Nuclear Physics PAN  
Radzikowskiego 152, 31-342 Kraków, Poland*

<sup>3</sup> *Centre de Physique Théorique, École Polytechnique,  
CNRS, 91128 Palaiseau, France*

<sup>4</sup> *Departamento de Física de Partículas and IGFAE,  
Universidad de Santiago de Compostela, 15782 Santiago de Compostela, Spain*

<sup>5</sup> *CERN PH-TH, CH-1211, Geneva 23, Switzerland*

## Abstract

We study forward dijet production in dilute-dense hadronic collisions. By considering the appropriate limits, we show that both the transverse-momentum-dependent (TMD) and the high-energy factorization formulas can be derived from the Color Glass Condensate framework. Respectively, this happens when the transverse momentum imbalance of the dijet system,  $k_t$ , is of the order of either the saturation scale, or the hard jet momenta, the former being always much smaller than the latter. We propose a new formula for forward dijets that encompasses both situations and is therefore applicable regardless of the magnitude of  $k_t$ . That involves generalizing the TMD factorization formula for dijet production to the case where the incoming small- $x$  gluon is off-shell. The derivation is performed in two independent ways, using either Feynman diagram techniques, or color-ordered amplitudes.

# 1 Introduction

Forward particle production observables in proton-proton (p+p) and proton-nucleus (p+A) collisions at the Large Hadron Collider (LHC) offer unique opportunities to study the dynamics of QCD at small  $x$ , and in particular the non-linear regime of parton saturation [1]. Indeed, in high-energy hadronic collisions, forward particle production is sensitive only to high-momentum partons inside one of the colliding hadrons, which therefore appears dilute. By contrast, for the other hadron or nucleus, it is mainly small-momentum partons, whose density is large, that contribute to the scattering. Such processes, in which a large- $x$  projectile is used as a probe to investigate a small- $x$  target, are sometimes called dilute-dense collisions. Since the high- $x$  part of the projectile wave function is well understood in perturbative QCD, forward particle production is indeed ideal to investigate the small- $x$  part of target wave function. This is true both in p+p and p+A collisions, although using a target nucleus does enhance the dilute-dense asymmetry of such collisions.

The separation between the linear and non-linear regimes of the target wave function is characterized by a momentum scale  $Q_s(x)$ , called the saturation scale, which increases as  $x$  decreases. Dilute-dense collisions can be described from first principles, provided  $Q_s \gg \Lambda_{\text{QCD}}$ . This condition is better realized with higher energies (as they open up the phase space towards lower values of  $x$ ), and with nuclear targets (since, roughly,  $Q_s \sim A^{1/3}$ ). Over the years, the Color Glass Condensate (CGC) effective theory [2] has emerged as the best candidate to approximate QCD in the saturation regime, both in terms of practical applicability and of phenomenological success [3]. In this paper, we focus on forward dijet production in p+A and p+p collisions. We note that the CGC approach has been very successful in describing forward di-hadron production at RHIC [4–6], in particular it predicted the suppression of azimuthal correlations in d+Au collisions compared to p+p collisions [7], which was observed later experimentally [8, 9].

With forward dijets at the LHC however, the full complexity of the CGC machinery is not needed. Indeed, for the di-hadron process at RHIC energies, no particular ordering of the momentum scales involved is assumed in CGC calculations, while, at the LHC, the presence of particles with transverse momenta much larger than the saturation scale clearly must imply some simplifications. On the flip side, there will be other complications since further QCD dynamics, which is not part of the CGC framework but which is relevant at large transverse momenta, must also be considered. There are three important momentum scales in the forward dijet process: a typical transverse momentum of a hard jet,  $P_t$ , whose precise definition will be stated in the next section; the transverse momentum of the small- $x$  gluons involved in the hard scattering,  $k_t$ ; and the saturation scale of the small- $x$  target,  $Q_s$ . Clearly,  $P_t$  is always one of the hardest scales, and it is much bigger than  $Q_s$ , which is always one of the softest scales. Then, depending on where  $k_t$  sits with respect to these two, three different regimes can be defined.

A first regime, with  $Q_s \ll k_t \sim P_t$ , corresponds to the domain of applicability of the so-called *high energy factorization* (HEF) framework [10, 11], in which the description of forward dijets involves an unintegrated gluon distribution for the small- $x$  target, along with off-shell hard matrix elements. That is explicitly shown in this work, starting from CGC calculations. While such a factorization does not occur when non-linear saturation effects are accounted for, we shall see that taking the  $Q_s \ll k_t \sim P_t$  limit is tantamount to restricting the interaction with the small- $x$  target to a two-gluon exchange, therefore allows to indeed write all the CGC correlators in terms of a single gluon distribution. Doing so, the matrix elements of the HEF framework are exactly recovered.

A second regime, with  $k_t \sim Q_s \ll P_t$ , is where the so-called *transverse momentum dependent* (TMD) factorization [12] is valid. It involves on-shell matrix elements but several unintegrated gluons distributions. In this regime, non-linear effects are present, and in the large- $N_c$

limit, equivalence with CGC expressions was shown in [13]. In particular, in that case the description of forward dijets involves only two independent unintegrated gluons distributions, each of which can be determined in various other processes [14]. In the present work we shall keep  $N_c$  finite, implying, as we show below, that a total of six independent unintegrated gluons distributions are needed.

Finally, the intermediate regime  $Q_s \ll k_t \ll P_t$ , which is naturally obtained from the two others by taking the appropriate limits, corresponds to the collinear regime, with on-shell matrix elements and the standard integrated gluon distribution.

Separately, the HEF and TMD approaches to dijet production have been extensively studied in the literature [11, 15–18] and [12, 19–25], but little connection has been made between them so far. The first result of this paper is to reveal that connection, in the context of dilute-dense collisions, and to show that, in fact, they are both contained in the CGC description. However, as already mentioned, using the CGC approach is unnecessarily complicated and one should take advantage of the fact that  $P_t \gg Q_s$  to simplify the theoretical formulation. The second result of the paper is precisely to develop a new formula for forward dijets in dilute-dense collisions that encompasses all three situations described above, meaning that it is applicable regardless of the magnitude of  $k_t$ . As explained below, this is obtained by extending the TMD factorization framework, more precisely by supplementing it with off-shell matrix elements.

Note that the derivation of our new unified formula is performed in two independent ways: first using the standard Feynman diagram technique, and second by exploiting the so-called helicity method that employs color-ordered amplitudes [26]. With this second method, the gauge invariance of the results is explicit, and the method will also prove very useful in the future, when processes with more particles in the final state are considered. As is the case in the CGC framework, our new formulation contains all the relevant limits, but it has the advantage that it is more amenable to phenomenological implementations than CGC calculations. In addition, it is also better suited to be supplemented with further QCD dynamics relevant at high  $P_t$ , such as Sudakov logarithms [27, 28] or coherence in the QCD evolution of the gluon density [29–31]. These tasks are left for future work.

The plan of the paper is as follows. In Section 2, we introduce kinematics and notations, and briefly present the HEF and TMD frameworks. In Section 3, we show that the HEF framework can be derived from CGC calculations, when the  $Q_s \ll k_t \sim P_t$  limit is considered; namely we explain how the various CGC correlators reduce to a single gluon distribution in that limit, and show that the off-shell matrix elements of the HEF framework are indeed emerging. Section 4 is devoted to the  $k_t \sim Q_s \ll P_t$  limit, the derivation of the TMD factorization formula for forward dijets given in [14] is recalled, and extended to the case of finite  $N_c$ , implying six independent unintegrated gluons distributions instead of two. The hard factors of the TMD framework are computed again in Section 5, but keeping the small- $x$  gluon off-shell, which leads us to our new unified formula for forward dijets in p+A collisions. In Section 6, both the TMD factorization formula and the off-shell hard factors are derived again, but using color-ordered amplitudes, instead of Feynman diagram techniques. Finally, Section 7 is devoted to conclusions and outlook.

## 2 Forward dijets in p+A collisions

We shall discuss the process of inclusive dijet production in the forward region, in collisions of dilute and dense systems

$$p(p_p) + A(p_A) \rightarrow j_1(p_1) + j_2(p_2) + X. \quad (2.1)$$

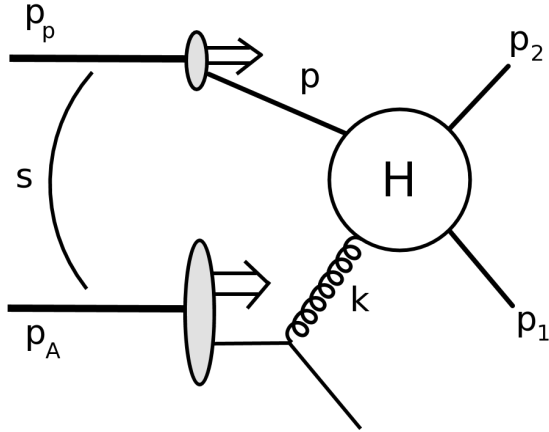


Figure 1: Inclusive dijet production in p+A collision. The blob  $H$  represents hard scattering. The solid lines coming out of  $H$  represent partons, which can be either quarks or gluons.

The process is shown schematically in Fig 1. The four-momenta of the projectile and the target are massless and purely longitudinal. In terms of the light cone variables,  $v^\pm = (v^0 \pm v^3)/\sqrt{2}$ , they take the simple form

$$p_p = \sqrt{\frac{s}{2}}(1, 0_t, 0), \quad p_A = \sqrt{\frac{s}{2}}(0, 0_t, 1), \quad (2.2)$$

where  $s$  is the squared center of mass energy of the p+A system.

The energy (or longitudinal momenta) fractions of the incoming parton (either a quark or gluon) from the projectile,  $x_1$ , and the gluon from the target,  $x_2$ , can be expressed in terms of the rapidities and transverse momenta of the produced jets as

$$x_1 = \frac{p_1^+ + p_2^+}{p_p^+} = \frac{1}{\sqrt{s}} (|p_{1t}|e^{y_1} + |p_{2t}|e^{y_2}), \quad (2.3a)$$

$$x_2 = \frac{p_1^- + p_2^-}{p_A^-} = \frac{1}{\sqrt{s}} (|p_{1t}|e^{-y_1} + |p_{2t}|e^{-y_2}), \quad (2.3b)$$

where  $p_{1t}, p_{2t}$  are transverse Euclidean two-vectors. By looking at jets produced in the forward direction, we effectively select those fractions to be  $x_1 \sim 1$  and  $x_2 \ll 1$ . Since the target A is probed at low  $x_2$ , the dominant contributions come from the subprocesses in which the incoming parton on the target side is a gluon

$$qg \rightarrow qg, \quad gg \rightarrow q\bar{q}, \quad gg \rightarrow gg. \quad (2.4)$$

In dilute-dense collisions, the large- $x$  partons of the dilute projectile are described in terms of the usual parton distribution functions of collinear factorization  $f_{a/p}$ , with a scale dependence given by DGLAP evolution equations. By contrast, the small- $x$  gluons of the dense target nucleus are described by a transverse-momentum-dependent distribution, which evolve towards small  $x$  according to non-linear equations. Moreover, the momentum  $k$  of the incoming gluon from the target, besides the longitudinal component  $k^- = x_2\sqrt{s/2}$ , has in general a non-zero transverse component,  $k_T$ , which leads to imbalance of transverse momentum of the produced jets

$$|k_t|^2 = |p_{1t} + p_{2t}|^2 = |p_{1t}|^2 + |p_{2t}|^2 + 2|p_{1t}||p_{2t}|\cos\Delta\phi, \quad (2.5)$$

with  $k_T^2 = -|k_t|^2$ . Here, by  $k_T$  we mean a four-vector, as opposed to  $k_t = p_{1t} + p_{2t}$ , which is a two-dimensional vector in the transverse plane. They are simply related by:  $k_T = (0, k_t, 0)$ . Using the notation defined above, the gluon's four-momentum can be also parametrized as

$$k = x_2 p_A + k_T. \quad (2.6)$$

The Mandelstam variables at the partonic level are defined as

$$\hat{s} = (p + k)^2 = (p_1 + p_2)^2 = \frac{|P_t|^2}{z(1-z)}, \quad (2.7a)$$

$$\hat{t} = (p_2 - p)^2 = (p_1 - k)^2 = -\frac{|p_{2t}|^2}{1-z}, \quad (2.7b)$$

$$\hat{u} = (p_1 - p)^2 = (p_2 - k)^2 = -\frac{|p_{1t}|^2}{z}, \quad (2.7c)$$

with

$$z = \frac{p_1^+}{p_1^+ + p_2^+} \quad \text{and} \quad P_t = (1-z)p_{1t} - zp_{2t}. \quad (2.8)$$

They sum up to  $\hat{s} + \hat{t} + \hat{u} = k_T^2$ .

Note that we always neglect the transverse momentum of the high- $x$  partons compared with that of the low- $x$  parton  $|k_t|$ . This is justified in view of the asymmetry of the problem,  $x_1 \sim 1$  and  $x_2 \ll 1$ , which implies that gluons from the target have a much bigger average transverse momentum (of the order of  $Q_s$ ) compared to that of the large  $x$  partons from the projectile (which of the order of  $\Lambda_{QCD}$ ). And even when the transverse momentum imbalance of the dijet system is of the same order as the jet transverse momenta themselves, implying that both parton distributions are probed in their radiative tail, the small  $x_2$  (BFKL) evolution implies a  $1/k_t$  behavior on the target side, while DGLAP evolution implies a  $1/k_t^2$  behavior on the projectile side.

To take into account small- $x$  effects in dijet production, an approach that has been broadly used in phenomenological studies involves the so-called high energy factorization (HEF) formula [15]

$$\frac{d\sigma^{pA \rightarrow \text{dijets}+X}}{dy_1 dy_2 d^2 p_{1t} d^2 p_{2t}} = \frac{1}{16\pi^3 (x_1 x_2 s)^2} \sum_{a,c,d} x_1 f_{a/p}(x_1, \mu^2) |\overline{\mathcal{M}}_{ag^* \rightarrow cd}|^2 \mathcal{F}_{g/A}(x_2, k_t) \frac{1}{1 + \delta_{cd}}. \quad (2.9)$$

This formula makes use of the unintegrated gluon distribution  $\mathcal{F}_{g/A}$  that is involved in the calculation of the deep inelastic structure functions. It is determined from fits to DIS data, and then used in Eq. (2.9), along with matrix elements that depend on the transverse momentum imbalance (2.5). Even though the high energy factorization is not strictly valid for dijet production, there exists a kinematic window, the dilute limit  $Q_s \ll |p_{1t}|, |p_{2t}|, |k_t|$ , in which it can be motivated from the CGC approach. We shall demonstrate this explicitly for all channels in the next section.

A second approach, valid in the regime where the transverse momentum imbalance between the outgoing particles, Eq. (2.5), is much smaller than their individual transverse momenta, is the so-called transverse momentum dependent (TMD) factorization. This limit,  $|p_{1t} + p_{2t}| \ll |p_{1t}|, |p_{2t}|$ , or  $|k_t| \ll |P_t|$ , corresponds to the situation of nearly back-to-back dijets. Even though, in general, there exists no TMD factorization theorem for jet production in hadron-hadron collisions, such a factorization can be established in the asymmetric ‘‘dilute-dense’’ situation considered here, where only one of the colliding hadrons is described by a transverse momentum

dependent gluon distribution. Again, selecting dijet systems produced in the forward direction implies  $x_1 \sim 1$  and  $x_2 \ll 1$ , which in turn allows us to make that assumption. The TMD factorization formula reads (so far, this has been obtained in the large- $N_c$  approximation, but this restriction will be lifted in the present work) [13]

$$\frac{d\sigma^{pA \rightarrow \text{dijets}+X}}{dy_1 dy_2 d^2p_{1t} d^2p_{2t}} = \frac{\alpha_s^2}{(x_1 x_2 s)^2} \sum_{a,c,d} x_1 f_{a/p}(x_1, \mu^2) \sum_i H_{ag \rightarrow cd}^{(i)} \mathcal{F}_{ag}^{(i)}(x_2, k_t) \frac{1}{1 + \delta_{cd}}, \quad (2.10)$$

where several unintegrated gluon distributions  $\mathcal{F}_{ag}^{(i)}$  with different operator definition are involved and accompanied by different hard factors  $H_{ag \rightarrow cd}^{(i)}$ . Those hard factors were calculated in [13] as if the small- $x_2$  gluon was on-shell (*i.e.*  $|k_t| = 0$ ). The  $k_t$  dependence survived only in the gluon distributions.

By restoring the  $k_t$  dependence of the hard factors inside formula (2.10), we can make the bridge between the HEF and TMD frameworks and obtain a unified formulation which encompasses both the dilute and the nearly back-to-back limit. Note that we follow the conventions used in earlier papers that dealt with these formalisms, such as Ref. [15] and [13] respectively. Therefore, contrary to the HEF matrix elements  $|\overline{\mathcal{M}}_{ag^* \rightarrow cd}|^2$ , the hard factors  $H_{ag \rightarrow cd}^{(i)}$  of the TMD factorization are defined without the  $g^4$  factor. In addition, the definition of the gluon distribution also differ by a factor  $\pi$ . The integrated gluon distribution  $x_2 f_{g/A}$  is obtained from  $\int dk_t^2 \mathcal{F}_{g/A}$  in the HEF formalism, and from  $\int d^2k_t \mathcal{F}_{ag}^{(i)}$  in the TMD formalism.

Finally, let us point out that, in the frameworks described above, one emits radiation in the transverse direction that one has no control over, as it is part of the small- $x$  gluon distributions and therefore is treated fully inclusively. To be more specific, at this level, transverse momentum conservation is obtained either by several particles of average transverse momentum  $Q_s$ , or by a third hard jet, depending on the magnitude of  $|k_t|$ . Due to the small- $x$  evolution, that radiation is ordered in rapidity, therefore it does not contribute to the measured forward dijets systems.

### 3 High energy factorization derived from CGC:

#### the $|p_{1t}|, |p_{2t}|, |k_t| \gg Q_s$ limit

We shall demonstrate that the high-energy factorization formula for double-inclusive particle production, Eq. (2.9), is identical to a result obtained from the CGC formalism in the dilute target approximation. This is a limit where all the momenta involved in the process are much larger than the saturation scale:  $|p_{1t}|, |p_{2t}|, |k_t| \gg Q_s$ . Here, we show explicitly the equivalence of the HEF and CGC formulas for the  $qg^* \rightarrow qg$  channel and only provide the final results for the two other channels, as the derivations proceed identically for all of them. We derive the CGC cross sections for the  $qg^* \rightarrow qg$  and  $gg^* \rightarrow q\bar{q}$  channels in the dilute limit following a procedure developed in Ref. [32] where only the  $gg^* \rightarrow gg$  sub-process was considered.

The amplitude for quark-gluon production is schematically presented in Fig. 2 as in Ref. [7]. In the left diagram, the emission of the gluon from the quark happens before the interaction with the target, and in the right diagram the emission occurs after the quark has interacted with the target. There is a relative minus sign between the two cases as explained in details in Ref. [7]. Multigluon interactions of quarks and gluons with a target, in the CGC formalism, enter as Wilson lines in the expression for the amplitude. A quark propagator is represented as a fundamental Wilson line, while a gluon propagator as an adjoint Wilson line. As a result, the cross section involves multipoint correlators of Wilson lines. In particular, the amplitude from Fig. 2, after squaring, has four terms: a correlator of four Wilson lines,  $S^{(4)}$ , corresponding to

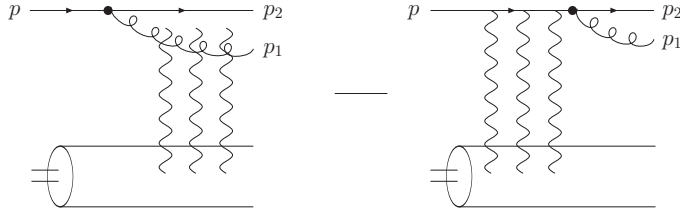


Figure 2: Amplitude for quark-gluon production in the CGC formalism. Left: the gluon is radiated before the interaction with the target. Right: the gluon is radiated after the interaction with the target. The two terms have a relative minus sign.

interactions happening after the emission of the gluon, both in the amplitude and the complex conjugate, then a correlator of two Wilson lines,  $S^{(2)}$ , representing the case when interactions with the target take place before the radiation of the gluon in both amplitude and complex conjugate, and two correlators of three Wilson lines,  $S^{(3)}$ , for the interference terms. In all the cases the splitting function is the same, and is given by the product of the quark wave functions:  $\phi_{\alpha\beta}^{\lambda*}(p, p_1^+, \mathbf{x}' - \mathbf{b}')\phi_{\alpha\beta}^\lambda(p, p_1^+, \mathbf{x} - \mathbf{b})$ . The total expression for the inclusive cross section in CGC is then given by the following formula [7]:

$$\frac{d\sigma(pA \rightarrow qgX)}{dy_1 dy_2 d^2 p_{1t} d^2 p_{2t}} = \alpha_s C_F (1-z) p_1^+ x_1 f_{q/p}(x_1, \mu^2) |\mathcal{M}(p, p_1, p_2)|^2, \quad (3.1)$$

where the amplitude squared,  $|\mathcal{M}(p, p_1, p_2)|^2$ , has the form:

$$\begin{aligned} |\mathcal{M}(p, p_1, p_2)|^2 &= \int \frac{d^2 \mathbf{x}}{(2\pi)^2} \frac{d^2 \mathbf{x}'}{(2\pi)^2} \frac{d^2 \mathbf{b}}{(2\pi)^2} \frac{d^2 \mathbf{b}'}{(2\pi)^2} e^{-ip_{1t} \cdot (\mathbf{x} - \mathbf{x}')} e^{-ip_{2t} \cdot (\mathbf{b} - \mathbf{b}')} \\ &\times \sum_{\lambda\alpha\beta} \phi_{\alpha\beta}^{\lambda*}(p, p_1^+, \mathbf{x}' - \mathbf{b}') \phi_{\alpha\beta}^\lambda(p, p_1^+, \mathbf{x} - \mathbf{b}) \\ &\times \left\{ S_{q\bar{q}g}^{(4)}[\mathbf{b}, \mathbf{x}, \mathbf{b}', \mathbf{x}'; x_2] - S_{q\bar{q}}^{(3)}[\mathbf{b}, \mathbf{x}, \mathbf{b}' + z(\mathbf{x}' - \mathbf{b}'); x_2] \right. \\ &\left. - S_{q\bar{q}}^{(3)}[\mathbf{b} + z(\mathbf{x} - \mathbf{b}), \mathbf{x}', \mathbf{b}'; x_2] + S_{q\bar{q}}^{(2)}[\mathbf{b} + z(\mathbf{x} - \mathbf{b}), \mathbf{b}' + z(\mathbf{x}' - \mathbf{b}'); x_2] \right\}, \quad (3.2) \end{aligned}$$

where  $\phi_{\alpha\beta}^\lambda$  are mixed-space quark wave functions and  $S^{(i)}$  are correlators of Wilson lines explained in details below. Following the notation from Fig. 1 and Eq. (2.8), we use the fraction of the plus components of four-momenta,  $z$ , with  $p_1$  being the four-momentum of the outgoing gluon and  $p_2$ , the four-momentum of the outgoing quark.

The fundamental,  $U(\mathbf{x})$ , and adjoint,  $V(\mathbf{x})$ , Wilson lines are defined as path-ordered exponentials of the gauge field (written here in the  $A^+ = 0$  gauge):

$$U(\mathbf{x}) = \mathcal{P} \exp \left[ ig \int dx^+ A_a^-(x^+, \mathbf{x}) t^a \right] \quad \text{and} \quad V(\mathbf{x}) = \mathcal{P} \exp \left[ ig \int dx^+ A_a^-(x^+, \mathbf{x}) T^a \right], \quad (3.3)$$

where  $t^a$  and  $T^a$  are the generators of the fundamental and adjoint representations of  $SU(N)$  respectively. The traces of products of Wilson lines appearing in the cross section are defined in the following way:

$$S_{q\bar{q}g}^{(4)}(\mathbf{b}, \mathbf{x}, \mathbf{b}', \mathbf{x}) = \frac{1}{C_F N_c} \left\langle \text{Tr} \left( U(\mathbf{b}) U^\dagger(\mathbf{b}') t^d t^c \right) \left[ V(\mathbf{x}) V^\dagger(\mathbf{x}') \right]^{cd} \right\rangle_{x_2}; \quad (3.4)$$

$$S_{q\bar{q}}^{(3)}(\mathbf{b}, \mathbf{x}, \mathbf{z}') = \frac{1}{C_F N_c} \left\langle \text{Tr} \left( U^\dagger(\mathbf{z}') t^c U(\mathbf{b}) t^d \right) V^{cd}(\mathbf{x}) \right\rangle_{x_2} ; \quad (3.5)$$

$$S_{q\bar{q}}^{(2)}(\mathbf{z}, \mathbf{z}') = \frac{1}{N_c} \left\langle \text{Tr} \left( U(\mathbf{z}) U^\dagger(\mathbf{z}') \right) \right\rangle_{x_2} . \quad (3.6)$$

The CGC average is taken over the background field evaluated at  $Y = \ln(1/x_2)$ . The product of wave functions in the massless limit is:

$$\sum_{\lambda\alpha\beta} \phi_{\alpha\beta}^{\lambda*}(p, p_1^+, \mathbf{u}') \phi_{\alpha\beta}^\lambda(p, p_1^+, \mathbf{u}) = \frac{8\pi^2}{p_1^+} \frac{\mathbf{u} \cdot \mathbf{u}'}{|\mathbf{u}|^2 |\mathbf{u}'|^2} (1 + (1-z)^2) . \quad (3.7)$$

Introducing a change of variables,  $\mathbf{u} = \mathbf{x} - \mathbf{b}$  and  $\mathbf{v} = z\mathbf{x} + (1-z)\mathbf{b}$  (and similar for the primed coordinates), we get [7]:

$$|\mathcal{M}(p, p_1, p_2)|^2 = \int \frac{d^2\mathbf{u}}{(2\pi)^2} \frac{d^2\mathbf{u}'}{(2\pi)^2} e^{iP_t \cdot (\mathbf{u}' - \mathbf{u})} \sum_{\lambda\alpha\beta} \phi_{\alpha\beta}^{\lambda*}(p, p_1^+, \mathbf{u}') \phi_{\alpha\beta}^\lambda(p, p_1^+, \mathbf{u}) \\ \times \int \frac{d^2\mathbf{v}}{(2\pi)^2} \frac{d^2\mathbf{v}'}{(2\pi)^2} e^{ik_t \cdot (\mathbf{v}' - \mathbf{v})} \left[ S_{q\bar{q}g}^{(4)}(\mathbf{b}, \mathbf{x}, \mathbf{b}', \mathbf{x}') - S_{q\bar{q}}^{(3)}(\mathbf{b}, \mathbf{x}, \mathbf{v}') - S_{q\bar{q}}^{(3)}(\mathbf{v}, \mathbf{x}', \mathbf{b}') + S_{q\bar{q}}^{(2)}(\mathbf{v}, \mathbf{v}') \right]. \quad (3.8)$$

The conjugate momentum to  $\mathbf{u}' - \mathbf{u}$  is  $P_t = (1-z)p_{1t} - zp_{2t}$ , and the one corresponding to  $\mathbf{v}' - \mathbf{v}$  is the total transverse momentum of the produced particles  $k_t = p_{1t} + p_{2t}$ . In terms of fundamental Wilson lines only:

$$S_{q\bar{q}g}^{(4)}(\mathbf{b}, \mathbf{x}, \mathbf{b}', \mathbf{x}') = \frac{1}{2C_F N_c} \left\langle \text{Tr} \left( U(\mathbf{b}) U^\dagger(\mathbf{b}') U(\mathbf{x}') U^\dagger(\mathbf{x}) \right) \text{Tr} \left( U(\mathbf{x}) U^\dagger(\mathbf{x}') \right) \right. \\ \left. - \frac{1}{N_c} \text{Tr} \left( U(\mathbf{b}) U^\dagger(\mathbf{b}') \right) \right\rangle_{x_2} , \quad (3.9)$$

and

$$S_{q\bar{q}}^{(3)}(\mathbf{b}, \mathbf{x}, \mathbf{v}') = \frac{1}{2C_F N_c} \left\langle \text{Tr} \left( U(\mathbf{b}) U^\dagger(\mathbf{x}) \right) \text{Tr} \left( U(\mathbf{x}) U^\dagger(\mathbf{v}') \right) - \frac{1}{N_c} \text{Tr} \left( U(\mathbf{b}) U^\dagger(\mathbf{v}') \right) \right\rangle_{x_2} . \quad (3.10)$$

In the dilute target limit we allow for only up to two gluon exchanges between the Wilson line propagators and the nucleus. Accordingly, we expand the Wilson lines to second order in the background field:

$$U(\mathbf{x}) \approx 1 + ig \int dx^+ A^-(x^+, \mathbf{x}) - \frac{g^2}{2} \int dx^+ dy^+ \mathcal{P} \{ A^-(x^+, \mathbf{x}) A^-(y^+, \mathbf{x}) \} + \mathcal{O}(A^3) . \quad (3.11)$$

To this order, the expectation values of the four- and three-point correlators are simply expressed in terms of the dipole operator  $S_{q\bar{q}}^{(2)}(\mathbf{v}, \mathbf{v}')$ . The dilute target approximation gives only a leading result in  $|\mathbf{v} - \mathbf{v}'|^2 Q_s^2$  for the expectation value of  $S_{q\bar{q}}^{(2)}(\mathbf{v}, \mathbf{v}')$ , which is equivalent to taking the limit  $|k_t| \gg Q_s$ . Similarly, when all the momenta involved in the process are much larger than the saturation scale, the correlators entering the cross section get the following expressions:

$$S_{q\bar{q}g}^{(4)}(\mathbf{b}, \mathbf{x}, \mathbf{b}', \mathbf{x}') = 1 - g^2 N_c \Gamma_{x_2}(\mathbf{x} - \mathbf{x}') - g^2 \frac{N_c^2 - 1}{2N_c} \Gamma_{x_2}(\mathbf{b} - \mathbf{b}') \\ - \frac{g^2 N_c}{2} [\Gamma_{x_2}(\mathbf{x} - \mathbf{b}) + \Gamma_{x_2}(\mathbf{x}' - \mathbf{b}') - \Gamma_{x_2}(\mathbf{x}' - \mathbf{b}) - \Gamma_{x_2}(\mathbf{x} - \mathbf{b}')] ; \quad (3.12)$$



$$S_{q\bar{q}}^{(3)}(\mathbf{b}, \mathbf{x}, \mathbf{v}') = 1 - \frac{g^2 N_c}{2} \Gamma_{x_2}(\mathbf{b} - \mathbf{x}) - \frac{g^2 N_c}{2} \Gamma_{x_2}(\mathbf{x} - \mathbf{v}') + \frac{g^2}{2N_c} \Gamma_{x_2}(\mathbf{b} - \mathbf{v}') ; \quad (3.13)$$

$$S_{q\bar{q}}^{(2)}(\mathbf{v}, \mathbf{v}') = 1 - g^2 \frac{N_c^2 - 1}{2N_c} \Gamma_{x_2}(\mathbf{v} - \mathbf{v}') . \quad (3.14)$$

In the above equations:

$$\Gamma_{x_2}(\mathbf{x} - \mathbf{y}) = \int dx^+ [\gamma_{x_2}(x^+, \mathbf{0}) - \gamma_{x_2}(x^+, \mathbf{r})] , \quad (3.15)$$

where  $\mathbf{r} = \mathbf{x} - \mathbf{y}$  and  $\gamma_{x_2}(x^+, \mathbf{r})$  is related to the expectation value of the two-field correlator:

$$\langle A_a^-(x^+, \mathbf{x}) A_b^-(y^+, \mathbf{y}) \rangle_{x_2} = \delta^{ab} \delta(x^+ - y^+) \gamma_{x_2}(x^+, \mathbf{x} - \mathbf{y}) . \quad (3.16)$$

Using the expressions for the multi-point functions  $S^{(i)}$ , we get the following result for the amplitude squared:

$$\begin{aligned} |\mathcal{M}(p, p_1, p_2)|^2 &= 4\pi^2 g^2 N_c (1 + (1 - z)^2) \frac{1}{p_1^+} \int \frac{d^2 \mathbf{u}}{(2\pi)^2} \frac{d^2 \mathbf{u}'}{(2\pi)^2} e^{iP_t \cdot (\mathbf{u}' - \mathbf{u})} \frac{\mathbf{u} \cdot \mathbf{u}'}{|\mathbf{u}|^2 |\mathbf{u}'|^2} \\ &\times \int \frac{d^2 \mathbf{v}}{(2\pi)^2} \frac{d^2 \mathbf{v}'}{(2\pi)^2} e^{ik_t \cdot (\mathbf{v}' - \mathbf{v})} \left[ \Gamma_{x_2}(\mathbf{x} - \mathbf{b}') + \Gamma_{x_2}(\mathbf{x}' - \mathbf{b}) + \Gamma_{x_2}(\mathbf{x} - \mathbf{v}') \right. \\ &\quad \left. + \Gamma_{x_2}(\mathbf{v} - \mathbf{x}') - 2\Gamma_{x_2}(\mathbf{x} - \mathbf{x}') - \frac{N_c^2 - 1}{N_c^2} \Gamma_{x_2}(\mathbf{b} - \mathbf{b}') \right. \\ &\quad \left. - \frac{N_c^2 - 1}{N_c^2} \Gamma_{x_2}(\mathbf{v} - \mathbf{v}') - \frac{1}{N_c^2} \Gamma_{x_2}(\mathbf{b} - \mathbf{v}') - \frac{1}{N_c^2} \Gamma_{x_2}(\mathbf{v} - \mathbf{b}') \right] . \quad (3.17) \end{aligned}$$

We perform the integrals in the above expression by changing the variables from  $\mathbf{v}$  and  $\mathbf{v}'$  to  $\mathbf{r}$  and  $\mathbf{B}$ . The integrals over the transverse distances of the type  $\mathbf{r} = \mathbf{v} - \mathbf{v}'$  are equivalent to the Fourier transform of Eq. (3.15) and give the unintegrated gluon distribution:

$$f_{x_2}(k_t) \equiv -k_t^2 \int d^2 \mathbf{r} \Gamma_{x_2}(\mathbf{r}) e^{-ik_t \cdot \mathbf{r}} = k_t^2 \int dx^+ \gamma_{x_2}(x^+, k_t) . \quad (3.18)$$

In our approximation, the correlators do not depend on the impact parameter  $\mathbf{B} = (\mathbf{v} + \mathbf{v}')/2$ . The integrals over  $\mathbf{B}$  factorize and give the transverse area of the target:  $\int d^2 \mathbf{B} = S_\perp$ . Finally, the rest two integrations reduce to:

$$\int d^2 \mathbf{u} e^{-iP_t \cdot \mathbf{u}} \frac{\mathbf{u}}{|\mathbf{u}|^2} = -2\pi i \frac{\mathbf{P}_t}{|\mathbf{P}_t|^2} . \quad (3.19)$$

In terms of the unintegrated gluon distribution, the amplitude squared then gets the form:

$$\begin{aligned} |\mathcal{M}(p, p_1, p_2)|^2 &= \frac{2}{(2\pi)^4} g^2 S_\perp N_c \frac{f_{x_2}(k_t)}{k_t^2} (1 + (1 - z)^2) \frac{1}{p_1^+} \\ &\times \left[ \frac{(N_c^2 - 1)}{2N_c^2} \frac{1}{P_t^2} + \frac{(N_c^2 - 1)}{2N_c^2} \frac{1}{p_{1t}^2} + \frac{1}{p_{2t}^2} + \frac{1}{N_c^2} \frac{P_t \cdot p_{1t}}{P_t^2 p_{1t}^2} + \frac{P_t \cdot p_{2t}}{P_t^2 p_{2t}^2} + \frac{p_{1t} \cdot p_{2t}}{p_{1t}^2 p_{2t}^2} \right] , \quad (3.20) \end{aligned}$$

We want to show that Eq. (3.20) reproduces the HEF formula (2.9) with the appropriate unintegrated parton distribution function and off-shell matrix elements. For this purpose, we need to find a relation between the unintegrated gluon distribution used in the above equation,  $f_{x_2}(k_t)$ , and  $\mathcal{F}_{g/A}(x_2, k_t)$ , which appears in the HEF formula (2.9). This is easily done by considering the deep inelastic scattering process, since  $\mathcal{F}_{g/A}(x_2, k_t)$  is precisely the unintegrated

gluon distribution involved in the formulation of the  $\gamma^* + A \rightarrow X$  total cross section, and is therefore related to the  $q\bar{q}$  dipole scattering amplitude in a straightforward manner (see for instance [16, 33]):

$$\mathcal{F}_{g/A}(x_2, k_t) = \frac{N_c}{\alpha_s(2\pi)^3} \int d^2\mathbf{v} d^2\mathbf{v}' e^{-ik_t \cdot (\mathbf{v} - \mathbf{v}')} \nabla_{\mathbf{v} - \mathbf{v}'}^2 \left[ 1 - S_{q\bar{q}}^{(2)}(\mathbf{v}, \mathbf{v}') \right]. \quad (3.21)$$

In the weak-field limit, using formula (3.14), this gives the relation

$$f_{x_2}(k_t) = \frac{4\pi^2}{S_\perp(N_c^2 - 1)} \mathcal{F}_{g/A}(x_2, k_t). \quad (3.22)$$

Then, the cross section for the  $qg$  production channel from Eq. (3.1) can be written in a more compact form

$$\frac{d\sigma(pA \rightarrow qgX)}{dy_1 dy_2 d^2p_{1t} d^2p_{2t}} = \frac{\alpha_s^2}{2\pi} x_1 f_{q/p}(x_1, \mu^2) z(1-z) \hat{P}_{gq}(z) \left[ 1 + \frac{(1-z)^2 p_{1t}^2}{P_t^2} - \frac{1}{N_c^2} \frac{z^2 p_{2t}^2}{P_t^2} \right] \frac{\mathcal{F}_{g/A}(x_2, k_t)}{p_{1t}^2 p_{2t}^2}, \quad (3.23)$$

where  $\hat{P}_{gq}(z)$  is related to the quark-to-gluon splitting function and is given by:

$$\hat{P}_{gq}(z) = \frac{1 + (1-z)^2}{z}. \quad (3.24)$$

It turns out that the above expression for the quark-gluon production cross section is identical to the result in the HEF formalism, Eq. (2.9), containing the off-shell amplitudes  $|\overline{\mathcal{M}}_{ag^* \rightarrow cd}|^2$ . The latter have been calculated in Refs. [11], [34] and [35].

The equivalence of the CGC and HEF formulas in the dilute limit can be shown in a similar way for the cross sections of the other two subprocesses,  $gg^* \rightarrow q\bar{q}$  and  $gg^* \rightarrow gg$ . The CGC results for the cross sections in this limit are:

$$\frac{d\sigma(pA \rightarrow q\bar{q}X)}{dy_1 dy_2 d^2p_{1t} d^2p_{2t}} = \frac{\alpha_s^2}{4C_F\pi} x_1 f_{g/p}(x_1, \mu^2) z(1-z) \hat{P}_{qg}(z) \left[ -\frac{1}{N_c^2} + \frac{(1-z)^2 p_{1t}^2 + z^2 p_{2t}^2}{P_t^2} \right] \frac{\mathcal{F}_{g/A}(x_2, k_t)}{p_{1t}^2 p_{2t}^2} \quad (3.25)$$

and [32]

$$\frac{d\sigma(pA \rightarrow ggX)}{dy_1 dy_2 d^2p_{1t} d^2p_{2t}} = \frac{\alpha_s^2 N_c}{\pi C_F} x_1 f_{g/p}(x_1, \mu^2) z(1-z) \hat{P}_{gg}(z) \left[ 1 + \frac{(1-z)^2 p_{1t}^2 + z^2 p_{2t}^2}{P_t^2} \right] \frac{\mathcal{F}_{g/A}(x_2, k_t)}{p_{1t}^2 p_{2t}^2}. \quad (3.26)$$

The expressions for  $\hat{P}_{qg}(z)$  and  $\hat{P}_{gg}(z)$  have the form:

$$\hat{P}_{qg}(z) = z^2 + (1-z)^2, \quad \hat{P}_{gg}(z) = \frac{z}{1-z} + \frac{1-z}{z} + z(1-z). \quad (3.27)$$

Again, Eqs. (3.25) and (3.26) are equivalent to the HEF formulas for the corresponding cross sections [16].

Therefore, in principle, the HEF formalism should not be employed to include non-linear effects, and one should stick to Balitsky-Fadin-Kuraev-Lipatov (BFKL) evolution [36–38], or Ciafaloni-Catani-Fiorani-Marchesini evolution [29–31], when evaluating the gluon distribution. In this spirit, most studies are performed using a gluon density evolved with an improved BFKL equation that includes some higher-order corrections [39], but no non-linear effects. However, we note that the HEF framework could be used with the Balitsky-Kovchegov (BK) equation [40, 41] in order to investigate the so-called geometric scaling regime, where saturation effects are felt, even though  $Q_s \ll k_t$ . The full saturation region,  $Q_s \sim k_t$ , is however, in principle, out of reach of formula (2.9). Along these lines, an estimate of saturation effects was obtained in [42, 43], using the BK equation extended to include the same higher-order corrections as included in the linear case [39].

## 4 TMD factorization for nearly back-to-back jets: the $|\mathbf{p}_{1t}|, |\mathbf{p}_{2t}| \gg |\mathbf{k}_t|, Q_s$ limit

In this section we discuss the special case of nearly back-to-back jets,  $|p_{1t} + p_{2t}| \ll |p_{1t}|, |p_{2t}|$ , where the differential cross section is given by formula (2.10). Several gluon distributions  $\mathcal{F}_{ag}^{(i)}$ , with different operator definition, are involved here. Indeed, as explained in [12], a generic unintegrated gluon distribution of the form

$$\mathcal{F}(x_2, k_t) \stackrel{\text{naive}}{=} 2 \int \frac{d\xi^+ d^2\xi}{(2\pi)^3 p_A^-} e^{ix_2 p_A^- \xi^+ - ik_t \cdot \xi} \langle A | \text{Tr} [F^{i-}(\xi^+, \xi) F^{i-}(0)] | A \rangle, \quad (4.1)$$

where  $F^{i-}$  are components of the gluon field strength tensor, must be also supplemented with gauge links, in order to render such a bi-local product of field operators gauge invariant.

The gauge links are path-ordered exponentials, with the integration path being fixed by the hard part of the process under consideration. Therefore, unintegrated gluon distributions are process-dependent.

In the following, we shall encounter two gauge links  $\mathcal{U}^{[+]}$  and  $\mathcal{U}^{[-]}$ , as well as the loop  $\mathcal{U}^{[\square]} = \mathcal{U}^{[+]} \mathcal{U}^{[-]\dagger} = \mathcal{U}^{[-]} \mathcal{U}^{[+]\dagger}$ . These links are composed of Wilson lines, their simplest expression is obtained in the  $A^+ = 0$  gauge:

$$\mathcal{U}^{[\pm]} = U(0, \pm\infty; \mathbf{0}) U(\pm\infty, \xi^+; \xi) \quad \text{with} \quad U(a, b; \mathbf{x}) = \mathcal{P} \exp \left[ ig \int_a^b dx^+ A_a^-(x^+, \mathbf{x}) t^a \right], \quad (4.2)$$

but the expressions of the various gluon distributions given below are gauge-invariant. From now on,  $F^{i-}(\xi^+, \xi)$  is simply denoted as  $F(\xi)$ , and the hadronic matrix elements  $\langle A | \dots | A \rangle \rightarrow \langle \dots \rangle$ . Note however that they are different from the CGC averages  $\langle \dots \rangle_{x_2}$  of the previous section. Indeed, the normalization of the hadronic state  $|A\rangle$  is defined as  $\langle A' | A \rangle = (2\pi)^3 2p_A^+ \delta(p_A^+ - p_A'^+) \delta^{(2)}(p_{At} - p_{At}')$ , while the CGC averages are normalized as  $\langle 1 \rangle_{x_2} = 1$ . As explained in [13], the two can be related by making the replacement  $\langle \dots \rangle_{x_2} \rightarrow \frac{\langle A | \dots | A \rangle}{\langle A | A \rangle}$ .

This approach to dijet production in proton-nucleus collisions was analyzed in Ref. [13]. The TMD factorization formula (2.10) was derived there in the large- $N_c$  limit, and shown to be equivalent to CGC calculations (*e.g.* formulas (3.1) and (3.2) in the case of the  $qA \rightarrow qg$  channel), after taking the limit  $|p_{1t}|, |p_{2t}| \gg |k_t|, Q_s$ . In this section, we derive the TMD factorization formula keeping  $N_c$  finite. We obtain corrections to the hard factors  $H_{ag \rightarrow cd}^{(i)}$  previously derived, and we calculate new hard factors corresponding to gluon distributions that were omitted before (as they were vanishing in the large- $N_c$  limit). The finite  $N_c$  extension prevents one to make a further simplification, called correlator factorization, essential to relate the TMD factorization and the CGC formalism, but gives completeness to the main result of this paper, *i.e.* the new factorization formula we propose below is valid for finite  $N_c$ . We also check explicitly the gauge invariance of these hard factors by computing them in a gauge different from the one used in [13].

An important fact to note is that, as a consequence of the  $|k_t| \ll |p_{1t}|, |p_{2t}|$  limit, the  $k_t$  dependence in (2.10) survives only in the gluon distributions, and the hard factors are calculated as if the small- $x_2$  gluon was on-shell. That is, looking at the hard partonic interaction represented by the blob  $H$  in Fig. 1,  $k^2 = -|k_t|^2$  is set to zero, and  $\hat{s} + \hat{t} + \hat{u} = 0$ .

### 4.1 The $qg \rightarrow qg$ channel

The complete set of independent cut diagrams contributing to this channel is shown in Fig. 3 (mirror images of diagrams (3), (5) and (6) give identical expressions).

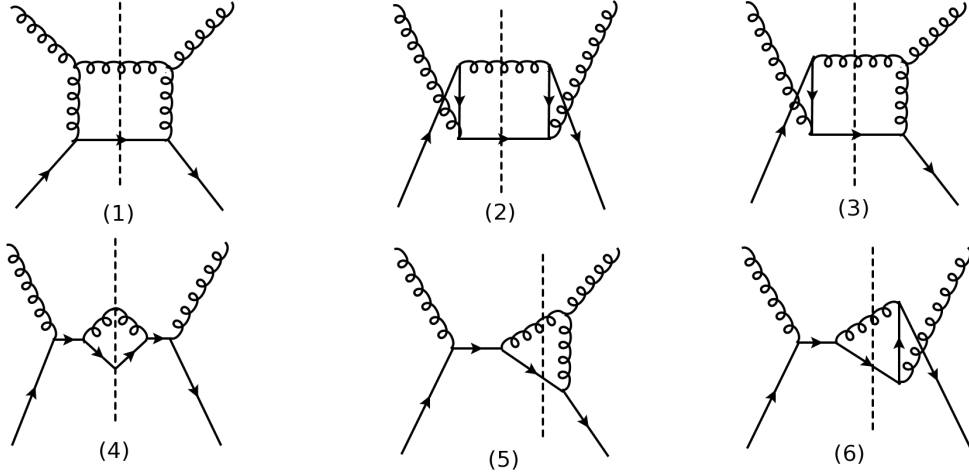


Figure 3: Diagrams for  $gg \rightarrow gg$  subprocess. The mirror diagrams of (3), (5) and (6) give identical contributions.

The cross section for a quark-gluon scattering involves only two different TMD gluon distributions as given in Ref. [12]:

$$\frac{d\sigma^{pA \rightarrow qgX}}{d^2P_t d^2k_t dy_1 dy_2} = \frac{\alpha_s^2}{(x_1 x_2 s)^2} x_1 f_{q/p}(x_1, \mu^2) \sum_{i=1}^2 \mathcal{F}_{qg}^{(i)} H_{qg \rightarrow qg}^{(i)}, \quad (4.3)$$

with:

$$\mathcal{F}_{qg}^{(1)} = 2 \int \frac{d\xi^+ d^2\xi}{(2\pi)^3 p_A^-} e^{ix_2 p_A^- \xi^+ - ik_t \cdot \xi} \left\langle \text{Tr} \left[ F(\xi) \mathcal{U}^{[-]\dagger} F(0) \mathcal{U}^{[+]} \right] \right\rangle = x_2 G^{(2)}(x_2, k_t), \quad (4.4)$$

$$\mathcal{F}_{qg}^{(2)} = 2 \int \frac{d\xi^+ d^2\xi}{(2\pi)^3 p_A^-} e^{ix_2 p_A^- \xi^+ - ik_t \cdot \xi} \left\langle \text{Tr} \left[ F(\xi) \frac{\text{Tr} [\mathcal{U}^{[\square]}]}{N_c} \mathcal{U}^{[+]\dagger} F(0) \mathcal{U}^{[+]} \right] \right\rangle. \quad (4.5)$$

These are the same gluon distributions as in the large- $N_c$  limit [13], no additional ones are present in this channel. The only difference in the expression (4.3) when we go to finite  $N_c$  will appear in the hard factor  $H_{qg \rightarrow qg}^{(1)}$  associated with  $\mathcal{F}_{qg}^{(1)}$ . That gluon distribution is sometimes also denoted  $x_2 G^{(2)}$ , and is called the *dipole distribution*, since it is the one that enters the formulation of the inclusive and semi-inclusive DIS.

In the CGC approach,  $x_2 G^{(2)}$  can be related to the  $q\bar{q}$  dipole scattering amplitude, and therefore linked to the gluon distribution used in the HEF formalism:  $\mathcal{F}_{g/A}(x_2, k_t) = \pi x_2 G^{(2)}(x_2, k_t)$ . That distribution is not sufficient however to compute the forward dijet cross section when  $|k_t| \sim Q_s$  (*i.e.* the case considered in this section). For completeness, we note that a detailed derivation of this relation between formula (3.21), involving a CGC correlation function, and formula (4.4), involving matrix elements defining TMDs, can be found in Appendix A of [13].

The exact results for the two hard factors read

$$H_{qg \rightarrow qg}^{(1)} = \frac{1}{2} D_1 - \frac{1}{N_c^2 - 1} D_2 + D_4 + 2D_5 + 2D_6, \quad (4.6)$$

$$H_{qg \rightarrow qg}^{(2)} = \frac{1}{2} D_1 + \frac{N_c}{2C_F} D_2 + 2D_3, \quad (4.7)$$

where  $D_i$ s are the squared and interference diagrams corresponding to the  $gg \rightarrow gg$  channel, following the numbering of Fig. 3. Each term  $D_i = C_{u_i} h_i$  represents the product of the color

factor,  $C_{u_i}$ , and the hard coefficient,  $h_i$ . What kind of diagrams enter the hard factors  $H_{qg \rightarrow qg}^{(i)}$  depends on the type of the gauge links appearing in each of them. As summarized in table IV of Ref. [12], the distribution  $\mathcal{F}_{qg}^{(1)}$  is present in diagrams (1), (2), (4), (5) and (6), while the distribution  $\mathcal{F}_{qg}^{(2)}$  appears in diagrams (1), (2) and (3). The  $D_i$  components were computed in Ref. [13] (table II) in an axial gauge with the axial vector,  $n$ , set to  $n = p$ , for both the incoming and the outgoing gluon, where  $p$  is the four-momentum of the incoming quark, as defined in Fig. 1. Formulated differently, the polarization vector of each external gluon was chosen such that, besides with the momentum of the gluon, their inner product with  $p$  vanishes. We recovered the same results for  $D_i$ s in that gauge and performed the same calculation in a different gauge with the axial vector set to  $n = p$  for the incoming gluon and  $n = p_2$  for the outgoing gluon <sup>1</sup>. The results for the hard factors  $H_{qg \rightarrow qg}^{(1)}$  and  $H_{qg \rightarrow qg}^{(2)}$  at finite  $N_c$  are identical in both gauges and they read

$$H_{qg \rightarrow qg}^{(1)} = -\frac{\hat{u}(\hat{s}^2 + \hat{u}^2)}{2\hat{s}\hat{t}^2} + \frac{1}{2N_c^2} \frac{(\hat{s}^2 + \hat{u}^2)}{\hat{s}\hat{u}}, \quad (4.8)$$

$$H_{qg \rightarrow qg}^{(2)} = -\frac{\hat{s}(\hat{s}^2 + \hat{u}^2)}{2\hat{u}\hat{t}^2}. \quad (4.9)$$

The hard factors and the TMDs entering the factorization formula (4.3) are all gauge invariant. In principle, that leaves us some freedom and the factorization formula can be rewritten with new hard factors and the corresponding new gluon distributions formed as linear combinations of the old ones.

For reasons that shall be discussed in detail in Section 6, let us define the new hard factors for the  $qg \rightarrow qg$  subprocess

$$K_{qg \rightarrow qg}^{(1)} = H_{qg \rightarrow qg}^{(1)} + \frac{1}{N_c^2} H_{qg \rightarrow qg}^{(2)} \quad \text{and} \quad K_{qg \rightarrow qg}^{(2)} = \frac{N_c^2 - 1}{N_c^2} H_{qg \rightarrow qg}^{(2)}, \quad (4.10)$$

and the corresponding new gluon TMDs

$$\Phi_{qg \rightarrow qg}^{(1)} = \mathcal{F}_{qg}^{(1)}, \quad (4.11)$$

$$\Phi_{qg \rightarrow qg}^{(2)} = \frac{1}{N_c^2 - 1} \left( -\mathcal{F}_{qg}^{(1)} + N_c^2 \mathcal{F}_{qg}^{(2)} \right), \quad (4.12)$$

such that the factorization formula (4.3) now takes the form

$$\frac{d\sigma^{pA \rightarrow qgX}}{d^2P_t d^2k_t dy_1 dy_2} = \frac{\alpha_s^2}{(x_1 x_2 s)^2} x_1 f_{q/p}(x_1, \mu^2) \left[ \Phi_{qg \rightarrow qg}^{(1)} K_{qg \rightarrow qg}^{(1)} + \Phi_{qg \rightarrow qg}^{(2)} K_{qg \rightarrow qg}^{(2)} \right]. \quad (4.13)$$

The explicit expressions for  $K_{qg \rightarrow qg}^{(1)}$  and  $K_{qg \rightarrow qg}^{(2)}$  are given in Table 1.

## 4.2 The $gg \rightarrow q\bar{q}$ channel

The independent cut diagrams contributing to this channel are shown in Fig. 4.

In addition to the two gluon distributions,  $\mathcal{F}_{gg}^{(1)}$  and  $\mathcal{F}_{gg}^{(2)}$ , used in Ref. [13], the result to all orders in  $N_c$  involves a third distribution [12, 44],  $\mathcal{F}_{gg}^{(3)}$  (also sometimes denoted  $x_2 G^{(1)}$  and called the *Weizsacker-Williams gluon distribution*), and the differential cross section reads

$$\frac{d\sigma^{pA \rightarrow q\bar{q}X}}{d^2P_t d^2k_t dy_1 dy_2} = \frac{\alpha_s^2}{(x_1 x_2 s)^2} x_1 f_{g/p}(x_1, \mu^2) \sum_{i=1}^3 \mathcal{F}_{gg}^{(i)} H_{gg \rightarrow q\bar{q}}^{(i)}, \quad (4.14)$$

---

<sup>1</sup>The choice of axial gauge vectors for external gluons corresponds to the choice of the reference momentum for their polarization vectors, see for example [26], and is arbitrary for gauge invariant quantities. Thus, the independence on those gauge vectors can be used to confirm that the result is gauge invariant.

	$K_{ag \rightarrow cd}^{(1)}$	$K_{ag \rightarrow cd}^{(2)}$
$qg \rightarrow qg$	$-\frac{\hat{s}^2 + \hat{u}^2}{2\hat{t}^2 \hat{s} \hat{u}} \left[ \hat{u}^2 + \frac{\hat{s}^2 - \hat{t}^2}{N_c^2} \right]$	$-\frac{C_F \hat{s}(\hat{s}^2 + \hat{u}^2)}{N_c \hat{t}^2 \hat{u}}$
$gg \rightarrow q\bar{q}$	$\frac{1}{2N_c} \frac{(\hat{t}^2 + \hat{u}^2)^2}{\hat{s}^2 \hat{t} \hat{u}}$	$-\frac{1}{2C_F N_c^2} \frac{\hat{t}^2 + \hat{u}^2}{\hat{s}^2}$
$gg \rightarrow gg$	$\frac{2N_c (\hat{s}^2 - \hat{t} \hat{u})^2 (\hat{t}^2 + \hat{u}^2)}{C_F \hat{t}^2 \hat{u}^2 \hat{s}^2}$	$\frac{2N_c (\hat{s}^2 - \hat{t} \hat{u})^2}{C_F \hat{t} \hat{u} \hat{s}^2}$

Table 1: The “new” hard factors following from simplified effective TMD factorization of Eqs. (4.13), (4.25) and (4.52) in the case with all partons being on shell.

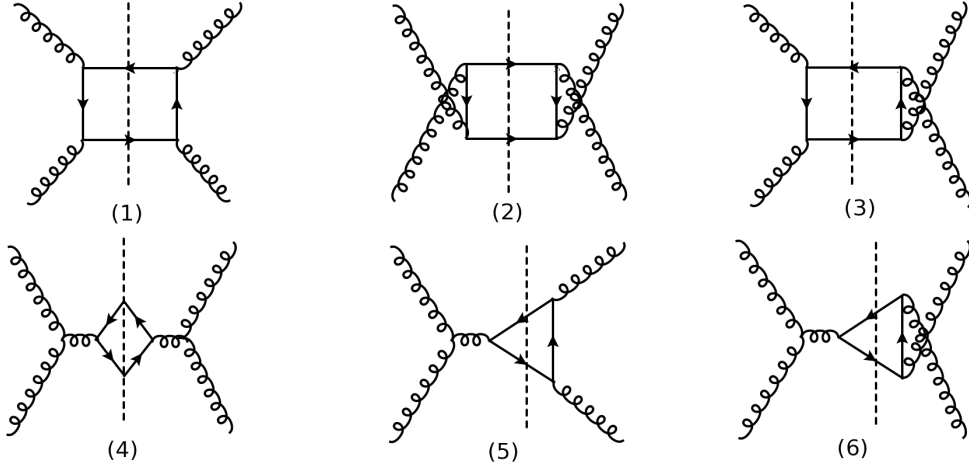


Figure 4: Diagrams for  $gg \rightarrow q\bar{q}$  subprocess. The mirror diagrams of (3), (5) and (6) give identical contributions.

with the three gluon TMDs defined as

$$\mathcal{F}_{gg}^{(1)} = 2 \int \frac{d\xi^+ d^2\xi}{(2\pi)^3 p_A^-} e^{ix_2 p_A^- \xi^+ - ik_t \cdot \xi} \left\langle \text{Tr} \left[ F(\xi) \frac{\text{Tr} [\mathcal{U}^{[\square]}]}{N_c} \mathcal{U}^{[-]\dagger} F(0) \mathcal{U}^{[+]} \right] \right\rangle, \quad (4.15)$$

$$\mathcal{F}_{gg}^{(2)} = 2 \int \frac{d\xi^+ d^2\xi}{(2\pi)^3 p_A^-} e^{ix_2 p_A^- \xi^+ - ik_t \cdot \xi} \frac{1}{N_c} \left\langle \text{Tr} \left[ F(\xi) \mathcal{U}^{[\square]\dagger} \right] \text{Tr} \left[ F(0) \mathcal{U}^{[\square]} \right] \right\rangle, \quad (4.16)$$

$$\mathcal{F}_{gg}^{(3)} = 2 \int \frac{d\xi^+ d^2\xi}{(2\pi)^3 p_A^-} e^{ix_2 p_A^- \xi^+ - ik_t \cdot \xi} \left\langle \text{Tr} \left[ F(\xi) \mathcal{U}^{[+]\dagger} F(0) \mathcal{U}^{[+]} \right] \right\rangle = x_2 G^{(1)}(x_2, k_t). \quad (4.17)$$

The appropriate hard factors are constructed from the expressions corresponding to the diagrams

(1)-(6) depicted in Fig. 4, using the following formulas

$$H_{gg \rightarrow q\bar{q}}^{(1)} = \frac{N_c}{2C_F} D_1 + \frac{N_c}{2C_F} D_2 + D_4 + 2D_5 + 2D_6, \quad (4.18)$$

$$H_{gg \rightarrow q\bar{q}}^{(2)} = -2N_c^2 D_3 - D_4 - 2D_5 - 2D_6, \quad (4.19)$$

$$H_{gg \rightarrow q\bar{q}}^{(3)} = -\frac{1}{N_c^2 - 1} D_1 - \frac{1}{N_c^2 - 1} D_2 + 2D_3. \quad (4.20)$$

Again, the components  $D_i = C_{u_i} h_i$  were computed in [13] (table III) and they were used there to determine the hard factors  $H_{gg \rightarrow q\bar{q}}^{(1,2)}$  in the large  $N_c$  limit. Here, we generalize the results of [13] to the full, finite- $N_c$  case. The calculation can be most readily done by exploiting crossing symmetry that relates the  $qg \rightarrow qg$  and  $gg \rightarrow q\bar{q}$  channels. This allows for identification of the diagrams between Figs. 3 and 4 and enables one to recycle the  $D_i$  expressions calculated in the previous subsection. For example, the expression corresponding to the diagram (1) from Fig. 4, with the incoming and the outgoing legs connected, is identical to the already computed expression for the diagram (4) from Fig. 3 (modulo a color averaging factor and swapping of the momenta  $p_1 \leftrightarrow p$ ). Similarly for all the other diagrams. That gives the following set of hard factors for the  $gg \rightarrow q\bar{q}$  subprocess:

$$H_{gg \rightarrow q\bar{q}}^{(1)} = \frac{1}{4C_F} \frac{(\hat{t}^2 + \hat{u}^2)^2}{\hat{s}^2 \hat{u} \hat{t}}, \quad (4.21)$$

$$H_{gg \rightarrow q\bar{q}}^{(2)} = \frac{1}{2C_F} \frac{\hat{t}^2 + \hat{u}^2}{\hat{s}^2}, \quad (4.22)$$

$$H_{gg \rightarrow q\bar{q}}^{(3)} = -\frac{1}{4N_c^2 C_F} \frac{\hat{t}^2 + \hat{u}^2}{\hat{t} \hat{u}}. \quad (4.23)$$

Of the three hard factors,  $H_{gg \rightarrow q\bar{q}}^{(i)}$ , only two are independent. The third hard factor,  $H_{gg \rightarrow q\bar{q}}^{(3)}$ , can be expressed as<sup>2</sup>

$$H_{gg \rightarrow q\bar{q}}^{(3)} = -\frac{1}{N_c^2} \left( H_{gg \rightarrow q\bar{q}}^{(1)} + H_{gg \rightarrow q\bar{q}}^{(2)} \right). \quad (4.24)$$

Therefore, the cross section for quark-antiquark production can be rewritten with only two hard factors and two gluon distributions that are linear combinations of  $\mathcal{F}_{gg}^{(1)}$ ,  $\mathcal{F}_{gg}^{(2)}$  and  $\mathcal{F}_{gg}^{(3)}$ :

$$\frac{d\sigma^{pA \rightarrow q\bar{q}X}}{d^2 P_t d^2 k_t dy_1 dy_2} = \frac{\alpha_s^2}{(x_1 x_2 s)^2} x_1 f_{g/p}(x_1, \mu^2) \left[ \Phi_{gg \rightarrow q\bar{q}}^{(1)} K_{gg \rightarrow q\bar{q}}^{(1)} + \Phi_{gg \rightarrow q\bar{q}}^{(2)} K_{gg \rightarrow q\bar{q}}^{(2)} \right]. \quad (4.25)$$

In the above, we defined the new gluon TMDs as

$$\Phi_{gg \rightarrow q\bar{q}}^{(1)} = \frac{1}{N_c^2 - 1} \left( N_c^2 \mathcal{F}_{gg}^{(1)} - \mathcal{F}_{gg}^{(3)} \right), \quad (4.26)$$

$$\Phi_{gg \rightarrow q\bar{q}}^{(2)} = -N_c^2 \mathcal{F}_{gg}^{(2)} + \mathcal{F}_{gg}^{(3)}, \quad (4.27)$$

and the hard factors  $K_{gg \rightarrow q\bar{q}}^{(i)}$  as:

$$K_{gg \rightarrow q\bar{q}}^{(1)} = \frac{N_c^2 - 1}{N_c^2} H_{gg \rightarrow q\bar{q}}^{(1)} \quad \text{and} \quad K_{gg \rightarrow q\bar{q}}^{(2)} = -\frac{1}{N_c^2} H_{gg \rightarrow q\bar{q}}^{(2)}. \quad (4.28)$$

The explicit expressions for the latter are given in Table 1.

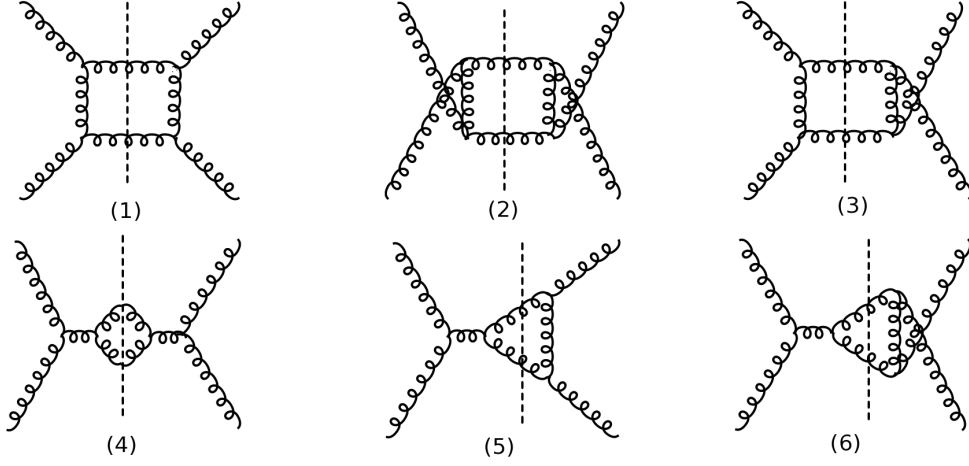


Figure 5: Set of diagrams for the  $gg \rightarrow gg$  subprocess involving only 3-gluon vertices. The mirror diagrams of (3), (5) and (6) give identical contributions.

### 4.3 The $gg \rightarrow gg$ channel

Finally, the independent cut diagrams for the  $gg \rightarrow gg$  channel are given in Figs. 5 and 6, and the corresponding differential cross section for two-gluon production reads:

$$\frac{d\sigma^{pA \rightarrow ggX}}{d^2P_t d^2k_t dy_1 dy_2} = \frac{\alpha_s^2}{(x_1 x_2 s)^2} x_1 f_{g/p}(x_1, \mu^2) \sum_{i=1}^6 \mathcal{F}_{gg}^{(i)} H_{gg \rightarrow gg}^{(i)}. \quad (4.29)$$

The  $\mathcal{F}_{gg}^{(1,2,3)}$  distributions are the same as the ones introduced in the previous section in Eqs. (4.15)-(4.17). The remaining three are [12]:

$$\mathcal{F}_{gg}^{(4)} = 2 \int \frac{d\xi^+ d^2\xi}{(2\pi)^3 p_A^-} e^{ix_2 p_A^- \xi^+ - ik_t \cdot \xi} \left\langle \text{Tr} \left[ F(\xi) \mathcal{U}^{[-]\dagger} F(0) \mathcal{U}^{[-]} \right] \right\rangle, \quad (4.30)$$

$$\mathcal{F}_{gg}^{(5)} = 2 \int \frac{d\xi^+ d^2\xi}{(2\pi)^3 p_A^-} e^{ix_2 p_A^- \xi^+ - ik_t \cdot \xi} \left\langle \text{Tr} \left[ F(\xi) \mathcal{U}^{[\square]\dagger} \mathcal{U}^{[+]\dagger} F(0) \mathcal{U}^{[\square]} \mathcal{U}^{[+]} \right] \right\rangle, \quad (4.31)$$

$$\mathcal{F}_{gg}^{(6)} = 2 \int \frac{d\xi^+ d^2\xi}{(2\pi)^3 p_A^-} e^{ix_2 p_A^- \xi^+ - ik_t \cdot \xi} \left\langle \text{Tr} \left[ F(\xi) \mathcal{U}^{[+]\dagger} F(0) \mathcal{U}^{[+]} \right] \frac{\text{Tr} [\mathcal{U}^{[\square]}]}{N_c} \frac{\text{Tr} [\mathcal{U}^{[\square]}]}{N_c} \right\rangle. \quad (4.32)$$

The associated hard factors are constructed as<sup>3</sup>:

$$H_{gg \rightarrow gg}^{(1)} = \frac{1}{2} D_1 + \frac{1}{2} D_2 + D_4 + 2D_5 + 2D_6, \quad (4.33)$$

$$H_{gg \rightarrow gg}^{(2)} = 2D_3 - D_4 - 2D_5 - 2D_6, \quad (4.34)$$

$$H_{gg \rightarrow gg}^{(6)} = -\frac{N_c^2}{2} H_{gg \rightarrow gg}^{(3)} = N_c^2 H_{gg \rightarrow gg}^{(4)} = N_c^2 H_{gg \rightarrow gg}^{(5)} = \frac{1}{2} D_1 + \frac{1}{2} D_2 + 2D_3. \quad (4.35)$$

The calculation of the  $gg \rightarrow gg$  subprocess requires inclusion of diagrams with four-gluon vertex. Therefore, in general, the expressions  $D_i$  in the above equations contain contributions

<sup>2</sup>The same relation holds of course already at the level of Eqs. (4.18)-(4.20).

<sup>3</sup>Note that what is called  $H_{gg \rightarrow gg}^{(3)}$  in Ref. [13] is now  $H_{gg \rightarrow gg}^{(6)}$ . Out of six hard factors, only  $H_{gg \rightarrow gg}^{(1)}$ ,  $H_{gg \rightarrow gg}^{(2)}$  and  $H_{gg \rightarrow gg}^{(6)}$  survive in the large- $N_c$  limit.



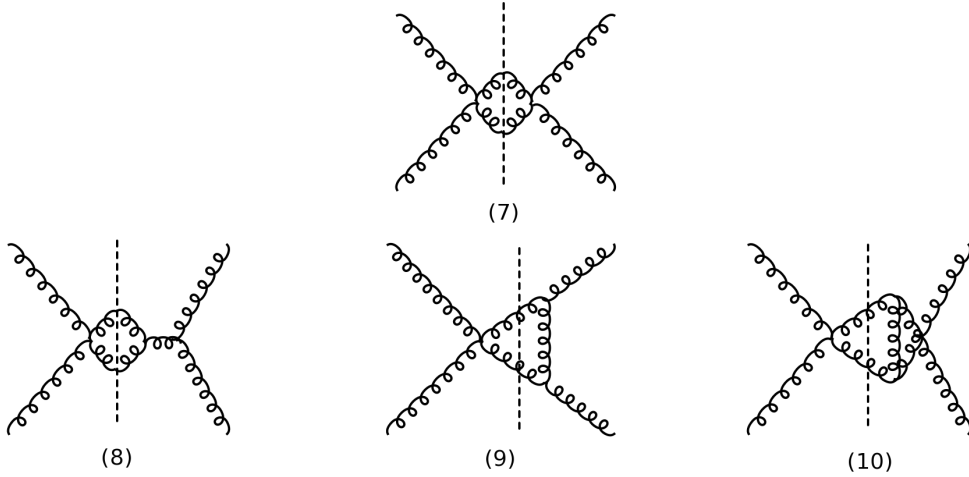


Figure 6: Set of diagrams for the  $gg \rightarrow gg$  subprocess involving 4-gluon vertex contributions. The mirror diagrams of (8), (9) and (10) give identical contributions.

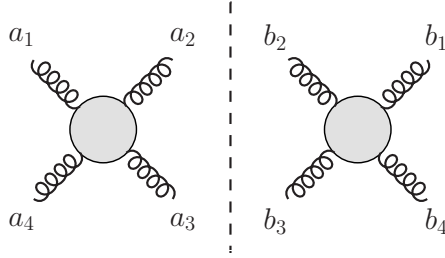


Figure 7: Color indices for the cut four-gluon squared matrix element.

from both, the 3-gluon and 4-gluon vertex diagrams, the latter shown in Fig. 6. The corresponding expressions were computed in [13], where they were used to determine the hard factors in the large- $N_c$  limit. Below, we generalize the result of Ref. [13] to the case of finite- $N_c$ , with the help of the exact definitions given in Eqs. (4.33)-(4.35). The six hard factors read

$$H_{gg \rightarrow gg}^{(1)} = \frac{N_c}{C_F} \frac{(\hat{t}^2 + \hat{u}^2)(\hat{s}^2 - \hat{t}\hat{u})^2}{\hat{u}^2 \hat{t}^2 \hat{s}^2}, \quad (4.36)$$

$$H_{gg \rightarrow gg}^{(2)} = \frac{2N_c}{C_F} \frac{(\hat{s}^2 - \hat{t}\hat{u})^2}{\hat{u}\hat{t}\hat{s}^2}, \quad (4.37)$$

$$H_{gg \rightarrow gg}^{(6)} = -\frac{N_c^2}{2} H_{gg \rightarrow gg}^{(3)} = N_c^2 H_{gg \rightarrow gg}^{(4)} = N_c^2 H_{gg \rightarrow gg}^{(5)} = \frac{N_c}{C_F} \frac{(\hat{s}^2 - \hat{t}\hat{u})^2}{\hat{u}^2 \hat{t}^2}. \quad (4.38)$$

To get further insight into the above results, we have performed an independent calculation in a gauge with non-vanishing 4-gluon vertex contribution, with the axial vectors defined as:

$$\begin{aligned} n = p & \quad \text{for the gluon } k, & n = k & \quad \text{for the gluon } p, \\ n = p_2 & \quad \text{for the gluon } p_1, & n = p_1 & \quad \text{for the gluon } p_2. \end{aligned} \quad (4.39)$$

The contributions to  $D_i$ s in this gauge, coming from diagrams with 3-gluon vertices only and depicted in Fig. 5, are given in Table 2.

	$h_i^{(3)}$	$C_i$
(1)	$\frac{4\hat{s}^6 + 4\hat{t}\hat{s}^5 + 17\hat{t}^2\hat{s}^4 + 36\hat{t}^3\hat{s}^3 + 24\hat{t}^4\hat{s}^2 + 8\hat{t}^5\hat{s} + 4\hat{t}^6}{\hat{s}^4\hat{t}^2}$	$\frac{N_c}{2C_F}$
(2)	$\frac{\hat{s}^6 + 2\hat{t}\hat{s}^5 + 33\hat{t}^2\hat{s}^4 + 60\hat{t}^3\hat{s}^3 + 44\hat{t}^4\hat{s}^2 + 16\hat{t}^5\hat{s} + 4\hat{t}^6}{\hat{s}^4(\hat{s} + \hat{t})^2}$	$\frac{N_c}{2C_F}$
(3)	$-\frac{2\hat{s}^6 - 9\hat{t}\hat{s}^5 + 19\hat{t}^2\hat{s}^4 + 48\hat{t}^3\hat{s}^3 + 4\hat{t}^4\hat{s}^2 - 24\hat{t}^5\hat{s} - 8\hat{t}^6}{2\hat{s}^4\hat{t}(\hat{s} + \hat{t})}$	$\frac{N_c}{4C_F}$
(4)	$\frac{(\hat{s} + 2\hat{t})^2}{\hat{s}^2}$	$\frac{N_c}{2C_F}$
(5)	$\frac{(\hat{s} + 2\hat{t})(2\hat{s}^3 - 3\hat{t}\hat{s}^2 - 2\hat{t}^2\hat{s} + 2\hat{t}^3)}{2\hat{s}^3\hat{t}}$	$\frac{N_c}{4C_F}$
(6)	$-\frac{(\hat{s} + 2\hat{t})(\hat{s}^3 - 7\hat{t}\hat{s}^2 - 8\hat{t}^2\hat{s} - 2\hat{t}^3)}{2\hat{s}^3(\hat{s} + \hat{t})}$	$-\frac{N_c}{4C_F}$

Table 2: Expressions for the  $gg \rightarrow gg$  subprocess corresponding to diagrams (1)-(6) of Fig. 5, hence containing only 3-gluon vertices, in gauge (4.39) with non-vanishing 4-gluon vertex contributions.

In order to add the 4-gluon vertex contribution and obtain a full result for the  $D_i$  coefficients, let us consider a general 4-gluon amplitude, shown on the left hand side of Fig. 7. A 3-gluon vertex brings a single  $SU(N)$  structure constant factor. Each amplitude in Fig. 5 consists of two 3-gluon vertices and that results in three possible color factor products

$$c_s \equiv f^{a_1 c a_4} f^{c a_2 a_3}, \quad c_t \equiv f^{a_1 a_2 c} f^{c a_3 a_4}, \quad c_u \equiv f^{a_1 a_3 c} f^{c a_4 a_2}, \quad (4.40)$$

for the amplitudes with a gluon exchange in the  $t$ -,  $s$ - and  $u$ -channels, respectively. Each of the above amplitudes can now be written as

$$\mathcal{M}_i^{3g} = c_i \mathcal{A}_i^{3g}, \quad (4.41)$$

where  $i$  is either  $t$ ,  $s$  or  $u$ ,  $c_i$  is a color factor from Eq. (4.40), and  $\mathcal{A}_i^{3g}$  is a corresponding kinematic expression. The  $3g$  superscript means that only 3-gluon vertices are involved in the given amplitude. Similarly, for the conjugate amplitudes, following the notation of Fig. 7, we have

$$\bar{c}_s \equiv f^{b_1 c b_4} f^{c b_2 b_3}, \quad \bar{c}_t \equiv f^{b_1 b_2 c} f^{c b_3 b_4}, \quad \bar{c}_u \equiv f^{b_1 b_3 c} f^{c b_4 b_2}. \quad (4.42)$$

That allows us to identify the color coefficients of the 3-gluon diagrams of Fig. 5 and write them in a compact form

$$\begin{aligned} (1) & \leftrightarrow c_t \bar{c}_t, & (2) & \leftrightarrow c_u \bar{c}_u, & (3) & \leftrightarrow c_t \bar{c}_u, \\ (4) & \leftrightarrow c_s \bar{c}_s, & (5) & \leftrightarrow c_s \bar{c}_t, & (6) & \leftrightarrow c_s \bar{c}_u. \end{aligned} \quad (4.43)$$

The  $\mathcal{O}(\alpha_s^2)$  contributions from diagrams with 4-gluon vertex are depicted in Fig. 6, where the first row shows the 4-gluon vertex amplitude squared, and the second row gives the interference

	$D_i$
(1)	$\frac{N_c (2\hat{s}^4 + 2\hat{s}^3\hat{t} + 3\hat{s}^2\hat{t}^2 + 8\hat{s}\hat{t}^3 + 6\hat{t}^4)}{C_F\hat{s}^2\hat{t}^2}$
(2)	$\frac{N_c (\hat{s}^4 + 4\hat{s}^3\hat{t} + 15\hat{s}^2\hat{t}^2 + 16\hat{s}\hat{t}^3 + 6\hat{t}^4)}{C_F\hat{s}^2(\hat{s} + \hat{t})^2}$
(3)	$-\frac{N_c (\hat{s}^4 + \hat{s}^3\hat{t} + 7\hat{s}^2\hat{t}^2 + 12\hat{s}\hat{t}^3 + 6\hat{t}^4)}{2C_F\hat{s}^2\hat{t}(\hat{s} + \hat{t})}$
(4)	$\frac{N_c(\hat{s} + 2\hat{t})^2}{C_F\hat{s}^2}$
(5)	$\frac{N_c(\hat{s} - 2\hat{t})(\hat{s} + \hat{t})(\hat{s} + 2\hat{t})}{2C_F\hat{s}^2\hat{t}}$
(6)	$-\frac{N_c \hat{t}(\hat{s} + 2\hat{t})(3\hat{s} + 2\hat{t})}{2C_F\hat{s}^2(\hat{s} + \hat{t})}$

Table 3: Full expressions for the diagrams including three-gluon and four-gluon vertex contributions in the gauge (4.39).

terms with the three types of  $\mathcal{M}^{3g}$  amplitudes from Eq. (4.41). A 4-gluon vertex amplitude contains all three color factor products of Eq. (4.40) at once

$$\mathcal{M}^{4g} = c_t \mathcal{A}_t^{4g} + c_s \mathcal{A}_s^{4g} + c_u \mathcal{A}_u^{4g}. \quad (4.44)$$

Therefore, all the contributions from Fig. 6 can be represented in the basis of the color factors defined in Eq. (4.43). This allows us to distribute all the pieces of diagrams from Fig. 6 over the six  $D_i$  expressions, needed to calculate the hard factors (4.33)-(4.35), according to their color factors. Hence, the full expressions are

$$D_1 = C_1 \left( h_1^{(3)} + 2\mathcal{A}_t^{4g} \mathcal{A}_t^{3g} + \mathcal{A}_t^{4g} \mathcal{A}_t^{4g} \right), \quad (4.45)$$

$$D_2 = C_2 \left( h_2^{(3)} + 2\mathcal{A}_u^{4g} \mathcal{A}_u^{3g} + \mathcal{A}_u^{4g} \mathcal{A}_u^{4g} \right), \quad (4.46)$$

$$D_3 = C_3 \left( h_3^{(3)} + \mathcal{A}_t^{4g} \mathcal{A}_u^{4g} + \mathcal{A}_t^{4g} \mathcal{A}_u^{3g} + \mathcal{A}_u^{4g} \mathcal{A}_t^{3g} \right), \quad (4.47)$$

$$D_4 = C_4 \left( h_4^{(3)} + 2\mathcal{A}_s^{4g} \mathcal{A}_s^{3g} + \mathcal{A}_s^{4g} \mathcal{A}_s^{4g} \right), \quad (4.48)$$

$$D_5 = C_5 \left( h_5^{(3)} + \mathcal{A}_t^{4g} \mathcal{A}_s^{4g} + \mathcal{A}_t^{4g} \mathcal{A}_s^{3g} + \mathcal{A}_s^{4g} \mathcal{A}_t^{3g} \right), \quad (4.49)$$

$$D_6 = C_6 \left( h_6^{(3)} + \mathcal{A}_s^{4g} \mathcal{A}_u^{4g} + \mathcal{A}_u^{4g} \mathcal{A}_s^{3g} + \mathcal{A}_s^{4g} \mathcal{A}_u^{3g} \right). \quad (4.50)$$

The results for  $D_i$ s in the gauge (4.39) are summarized in in Table 3. Plugging those expressions into the hard factor definitions (4.33)-(4.35) leads to the results identical to Eqs. (4.36)-(4.38).

We have already seen that not all of the six hard factors that arise in the  $gg \rightarrow gg$  subprocess are independent. As shown in Eq. (4.35), the expressions for  $H_{gg \rightarrow gg}^{(3)}$ ,  $H_{gg \rightarrow gg}^{(4)}$ ,  $H_{gg \rightarrow gg}^{(5)}$  and  $H_{gg \rightarrow gg}^{(6)}$  differ only by numerical factors. On top of that, when examining further Eqs. (4.33),

(4.34) and (4.35), we see that the hard factors  $H_{gg \rightarrow gg}^{(1)}$ ,  $H_{gg \rightarrow gg}^{(2)}$  and  $H_{gg \rightarrow gg}^{(6)}$  are linearly dependent, that is

$$H_{gg \rightarrow gg}^{(6)} = H_{gg \rightarrow gg}^{(1)} + H_{gg \rightarrow gg}^{(2)}. \quad (4.51)$$

Hence, the cross section for two-gluon production from Eq. (4.29) can be written in a much simpler, factorized form, with only two hard factors and two gluon distributions

$$\frac{d\sigma^{pA \rightarrow ggX}}{d^2P_t d^2k_t dy_1 dy_2} = \frac{\alpha_s^2}{(x_1 x_2 s)^2} x_1 f_{g/p}(x_1, \mu^2) \left[ \Phi_{gg \rightarrow gg}^{(1)} K_{gg \rightarrow gg}^{(1)} + \Phi_{gg \rightarrow gg}^{(2)} K_{gg \rightarrow gg}^{(2)} \right]. \quad (4.52)$$

In this channel, the new gluon TMDs,  $\Phi_{gg \rightarrow gg}$ , are defined as the following linear combinations of  $\mathcal{F}_{gg}^{(1)}$ ,  $\mathcal{F}_{gg}^{(2)}$ ,  $\dots$ ,  $\mathcal{F}_{gg}^{(6)}$ :

$$\Phi_{gg \rightarrow gg}^{(1)} = \frac{1}{2} \left( \mathcal{F}_{gg}^{(1)} - \frac{2}{N_c^2} \mathcal{F}_{gg}^{(3)} + \frac{1}{N_c^2} \mathcal{F}_{gg}^{(4)} + \frac{1}{N_c^2} \mathcal{F}_{gg}^{(5)} + \mathcal{F}_{gg}^{(6)} \right), \quad (4.53)$$

$$\Phi_{gg \rightarrow gg}^{(2)} = \mathcal{F}_{gg}^{(2)} - \frac{2}{N_c^2} \mathcal{F}_{gg}^{(3)} + \frac{1}{N_c^2} \mathcal{F}_{gg}^{(4)} + \frac{1}{N_c^2} \mathcal{F}_{gg}^{(5)} + \mathcal{F}_{gg}^{(6)}, \quad (4.54)$$

and the new hard factors are:

$$K_{gg \rightarrow gg}^{(1)} = 2H_{gg \rightarrow gg}^{(1)}, \quad \text{and} \quad K_{gg \rightarrow gg}^{(2)} = H_{gg \rightarrow gg}^{(2)}. \quad (4.55)$$

The explicit expressions are given in Table 1. We note, that the above simplification occurs naturally when utilizing gauge invariance from the start, as we will show in section 6.

Finally, we point out that, in the large- $N_c$  limit, all the distributions that were introduced in this section,  $\mathcal{F}_{qg}^{(1)}$ ,  $\mathcal{F}_{qg}^{(2)}$ ,  $\mathcal{F}_{gg}^{(1)}$ ,  $\mathcal{F}_{gg}^{(2)}$ , and  $\mathcal{F}_{gg}^{(6)}$ , can be written in terms of  $xG^{(1)}$  and  $xG^{(2)}$ , and equivalence of formulas (4.13), (4.25) and (4.52) with CGC results is obtained [13].

Let us conclude that this part of our work brings two improvements to the current state of the art for the TMD factorization in forward dijet production. First of all, we have obtained finite- $N_c$  corrections to the hard factors of Ref. [13]. More importantly, however, we have eliminated the redundancy in the number of gluon distributions needed to write a factorization formula for this process, which now takes the compact form

$$\frac{d\sigma^{pA \rightarrow \text{dijets}+X}}{d^2P_t d^2k_t dy_1 dy_2} = \frac{\alpha_s^2}{(x_1 x_2 s)^2} \sum_{a,c,d} x_1 f_{a/p}(x_1, \mu^2) \sum_{i=1}^2 K_{ag \rightarrow cd}^{(i)} \Phi_{ag \rightarrow cd}^{(i)} \frac{1}{1 + \delta_{cd}}, \quad (4.56)$$

with only two gluon distributions and two hard factors required in each channel. Note that, as we shall discuss now, the incoming, small- $x$  gluon is kept on-shell. Eqs. (4.56) will be further generalized to the case of the off-shell gluon in Section 5.

#### 4.4 The $|k_t| \gg Q_s$ limit

Finally, let us consider the limit  $|k_t| \gg Q_s$ . This is the dilute limit considered in Section 3, with the extra requirement that  $|k_t| \ll |P_t|$ , needed for the validity of those formula. In that limit, the transverse separation between the field operators in the definition of the gluon distribution is restricted to values much smaller than the distance over which the Fourier integrand varies, and the  $\xi$  dependence of the gauge links can be neglected. As a result, they simplify, and all the  $\mathcal{F}_{ag}^{(i)}$  distributions coincide, except  $\mathcal{F}_{gg}^{(2)}$  which vanishes. In terms of the  $\Phi_{ag \rightarrow cd}^{(1,2)}$  functions, all six distributions also reduce to that one gluon distribution, which can therefore be identified with  $\mathcal{F}_{g/A}/\pi$ .

Then, for all channels, one can easily sum the surviving hard factors. In terms of diagrams, we always obtain  $D_1 + D_2 + 2D_3 + D_4 + 2D_5 + 2D_6$ , meaning that we recover the collinear matrix elements. Indeed we have (noting that  $H_{gg \rightarrow gg}^{(3)} + H_{gg \rightarrow gg}^{(4)} + H_{gg \rightarrow gg}^{(5)} = 0$ ):

$$H_{qg \rightarrow qg}^{(1)} + H_{qg \rightarrow qg}^{(2)} = K_{qg \rightarrow qg}^{(1)} + K_{qg \rightarrow qg}^{(2)} = \frac{\hat{s}^2 + \hat{u}^2}{\hat{t}^2} - \frac{C_F}{N_c} \frac{\hat{s}^2 + \hat{u}^2}{\hat{s}\hat{u}} = \frac{1}{g^4} |\overline{\mathcal{M}}_{qg \rightarrow qg}|^2, \quad (4.57)$$

$$H_{gg \rightarrow q\bar{q}}^{(1)} + H_{gg \rightarrow q\bar{q}}^{(3)} = K_{gg \rightarrow q\bar{q}}^{(1)} + K_{gg \rightarrow q\bar{q}}^{(2)} = \frac{1}{2N_c} \frac{\hat{t}^2 + \hat{u}^2}{\hat{t}\hat{u}} - \frac{1}{2C_F} \frac{\hat{t}^2 + \hat{u}^2}{\hat{s}^2} = \frac{1}{g^4} |\overline{\mathcal{M}}_{gg \rightarrow q\bar{q}}|^2, \quad (4.58)$$

$$H_{gg \rightarrow gg}^{(1)} + H_{gg \rightarrow gg}^{(6)} = K_{gg \rightarrow gg}^{(1)} + K_{gg \rightarrow gg}^{(2)} = \frac{2N_c}{C_F} \frac{(\hat{s}^2 - \hat{t}\hat{u})^3}{\hat{s}^2 \hat{t}^2 \hat{u}^2} = \frac{1}{g^4} |\overline{\mathcal{M}}_{gg \rightarrow gg}|^2. \quad (4.59)$$

Therefore, we recover the HEF formula (2.9), except that, due to the  $|k_t| \ll |P_t|$  limit, the matrix elements are on-shell: the transverse momentum of the incoming gluon,  $k_t$ , survives only in  $\mathcal{F}_{g/A}$ . In other words, we recover the standard high- $|P_t|$  limit:

$$\frac{d\sigma^{pA \rightarrow \text{dijets}+X}}{dy_1 dy_2 dP_t^2 dk_t^2} = \sum_{a,c,d} \frac{1}{1 + \delta_{cd}} x_1 f_{a/p}(x_1, \mu^2) \frac{d\hat{\sigma}_{ag \rightarrow cd}}{d\hat{t}} \mathcal{F}_{g/A}(x_2, k_t), \quad (4.60)$$

with  $d\hat{\sigma}_{ag \rightarrow cd}/d\hat{t} = |\overline{\mathcal{M}}_{ag \rightarrow cd}|^2/[16\pi(x_1 x_2 s)^2]$ , and where  $\mathcal{F}_{g/A}(x_2, k_t)$  can be identified with  $\partial/\partial k_t^2 x_2 f_{g/A}(x_2, k_t^2)$ , the derivative of the integrated gluon distribution.

In the following section, we shall restore the  $k_t$  dependence of the hard factors. This will extend our formulas such that they recover the full HEF formula when the dilute limit is considered. As a result, we will obtain a unified description, valid for generic forward dijet system with  $|p_{1t}|, |p_{2t}| \gg Q_s$ , without any additional requirement on the magnitude of the transverse momentum imbalance  $k_t$ .

## 5 Unified description of forward dijets in p+A collisions: TMD factorization with off-shell hard factors

We shall now generalize the hard factors that enter the TMD factorization formula (2.10) to the case with one of the incoming gluons being off the mass shell, as illustrated in Fig. 8. As it has been already stated, the motivation to include the offshellness is to be able to allow for configurations where the dijets are produced at any azimuthal angle (of course before application of a jet algorithm that will suppress very small angles and hence render the results finite).

As can be seen in Fig. 9 (as an example we chose only purely gluonic matrix element but the same structure occurs for the other channels), the on-shell matrix element misses substantial contributions when the jets are produced at small angles near  $\Delta\phi = 0$  and at small rapidity differences  $\Delta Y = |y_1 - y_2| \simeq 0$ . In such configurations, the matrix element develops a structure that is divergent and it is suppressed only by a jet algorithm, which has to be applied in order to ensure two-jet configurations [16]. The matrix elements squared we are after, *i.e.*  $gg^* \rightarrow gg$ ,  $gg^* \rightarrow q\bar{q}$  and  $qg^* \rightarrow qg$ , can be extracted from the high energy limit (or eikonal limit) of  $qg \rightarrow qgg$  and  $qg \rightarrow q\bar{q}q$  and  $qq' \rightarrow qq'g$  [35]. In this approach the quark  $q$  is an auxiliary line to which the initial state off-shell gluon  $g^*$  couples eikonally.

The high energy factorization is a direct procedure where one uses the standard Feynman rules for all vertices and color factors, and fixes the light-cone gauge for the on-shell gluons, using a gauge vector given by the longitudinal component of the off-shell, initial-state gluon's momentum. In particular, if we apply the high energy factorization to the process we are after, we set the gauge vector to  $n = p_A$ , where  $p_A$  is the target four-momentum, as defined in Fig. 1 and Eq. (2.2). Furthermore, the prescription is to associate with the off-shell gluon a longitudinal

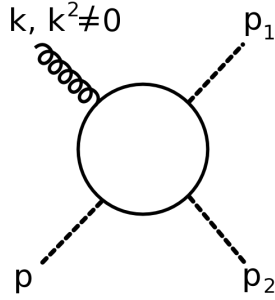


Figure 8: Four-parton amplitude with the incoming, small- $x$ , off-shell gluon.

polarization vector, called *nonsense polarization* [1], of the form <sup>4</sup>

$$\epsilon_\mu^0 = \frac{i\sqrt{2}x_2}{|k_t|} p_{A\mu}. \quad (5.1)$$

As elaborated in Ref. [10], longitudinally polarized gluons provide the dominant contribution to the cross section in the high energy limit. In the square amplitude, this leads to the polarization tensor of the form [10]

$$\epsilon_\mu^0 \epsilon_\nu^{0*} = \frac{-2x_2^2}{k^2} p_{A\mu} p_{A\nu}, \quad (5.2)$$

In the above,  $x_2 = k_\mu p^\mu / p_{A\nu} p^\nu$ , which follows directly from the definition in Eq. (2.6). The sum over polarizations of the on-shell gluons takes the standard form, with the gauge vector given by  $p_A$

$$\sum_{\lambda=\pm} \epsilon_\mu^\lambda \epsilon_\nu^{\lambda*} = g_{\mu\nu} - \frac{p_{A\mu} q_\nu + q_\mu p_{A\nu}}{q^\rho p_{A\rho}}, \quad (5.3)$$

where, depending on the channel,  $q = p, p_1$  or  $p_2$ , *c.f.* Eq. (4.39).

Let us note that the procedure outlined above defines the hard process in a gauge invariant manner only when a special choice for polarization vectors of the on-shell gluons is taken. In an arbitrary gauge, for internal and external gluon lines, more sophisticated methods have to be used, see *e.g.* [35, 45–48].

To present our results in a compact form, with direct relation to the on-shell formulas from Section 4, in addition to the standard Mandelstam variables given by Eqs. (2.7), which now, however, sum up to  $\hat{s} + \hat{t} + \hat{u} = k_T^2$ , we introduce their barred versions, defined only with the longitudinal component of the off-shell gluon

$$\bar{s} = (x_2 p_A + p)^2 = \frac{|P_t|^2}{z(1-z)} + |k_t|^2 = x_1 x_2 s, \quad (5.4a)$$

$$\bar{t} = (x_2 p_A - p_1)^2 = -z \bar{s}, \quad (5.4b)$$

$$\bar{u} = (x_2 p_A - p_2)^2 = -(1-z) \bar{s}, \quad (5.4c)$$

which are related via the equation

$$\bar{s} + \bar{t} + \bar{u} = 0. \quad (5.5)$$

<sup>4</sup>The  $\sqrt{2}$  factor in Eq. (5.1) follows from a convention. It allows for use of the on-shell-like factor  $\frac{1}{2}$  in averaging over polarization, while calculating matrix elements squared, even in the case of the off-shell gluon, where the actual number of polarizations in the high energy limit is 1.

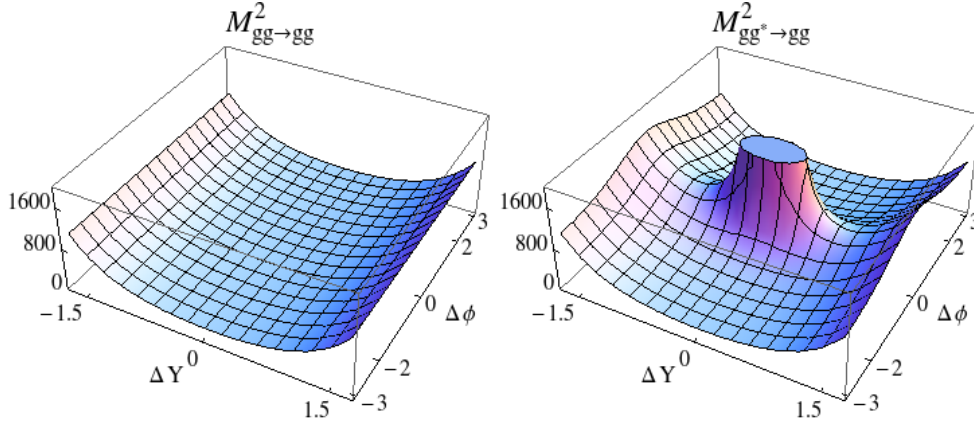


Figure 9: Matrix elements squared for  $gg \rightarrow gg$  scattering with  $p_{t1} = p_{t2} = 4$  GeV and  $\alpha_s = 0.2$ . Left: the on-shell case. Right: the off-shell case.  $\Delta Y$  and  $\Delta \phi$  are, respectively, the differences in rapidity and azimuthal angle of the two outgoing gluons.

In the on-shell limit,  $k_T^2 \rightarrow 0$ , the variables defined above recover the standard Mandelstam variables from Eq. (2.7)

$$\lim_{|k_t| \rightarrow 0} (\bar{s} - \hat{s}) = 0, \quad \lim_{|k_t| \rightarrow 0} (\bar{t} - \hat{t}) = 0, \quad \lim_{|k_t| \rightarrow 0} (\bar{u} - \hat{u}) = 0. \quad (5.6)$$

As a consistency check, we have verified that, for all three subprocesses, the off-shell amplitudes that shall be used to build the hard factors in the remaining part of this section are identical to those first calculated in Ref. [11].

From this point onwards, we shall discuss our results only in terms of the new  $K^{(i)}$  hard factors and the new factorization formulas from Eqs. (4.13), (4.25) and (4.52). The results for the old hard factors,  $H^{(i)}$ , in the off-shell case are given in Appendix A for completeness.

### 5.1 The $qg^* \rightarrow qg$ channel

The off-shell hard factors for this channel are obtained using definitions given in Eq. (4.10) and then Eqs. (4.6) and (4.7). The corresponding  $D_i$  expressions are collected in Appendix A in Table 8. The two hard factors read

$$K_{qg^* \rightarrow qg}^{(1)} = -\frac{\bar{s}^2 + \bar{u}^2}{2\hat{t}\hat{s}\hat{u}} \left[ \bar{u}\hat{u} + \frac{\bar{s}\hat{s} - \bar{t}\hat{t}}{N_c^2} \right], \quad (5.7)$$

$$K_{qg^* \rightarrow qg}^{(2)} = -\frac{C_F}{N_c} \frac{\bar{s}(\bar{s}^2 + \bar{u}^2)}{\bar{t}\hat{t}\hat{u}}. \quad (5.8)$$

In the limit  $|k_t| \rightarrow 0$ , simplification given by Eq. (5.6) occurs and the above formulas manifestly recover the on-shell results from Table 1.

### 5.2 The $gg^* \rightarrow q\bar{q}$ channel

The off-shell hard factors are obtained using definitions given in Eq. (4.28) and then Eqs. (4.18), (4.19) and (4.20). The corresponding  $D_i$  expressions are collected in Appendix A in Table 9.

The two hard factors take the following compact form

$$K_{gg^* \rightarrow q\bar{q}}^{(1)} = \frac{1}{2N_c} \frac{\bar{t}^2 + \bar{u}^2}{\bar{s}\hat{s}\hat{t}\hat{u}} [\bar{u}\hat{u} + \bar{t}\hat{t}] , \quad (5.9)$$

$$K_{gg^* \rightarrow q\bar{q}}^{(2)} = \frac{1}{4N_c^2 C_F} \frac{\bar{t}^2 + \bar{u}^2}{\bar{s}\hat{s}\hat{t}\hat{u}} [\bar{u}\hat{u} + \bar{t}\hat{t} - \bar{s}\hat{s}] . \quad (5.10)$$

Again, following Eq. (5.6), it is manifest that the above hard factors reduce to those given in Table 1, in the limit  $|k_t| \rightarrow 0$ .

### 5.3 The $gg^* \rightarrow gg$ channel

In the gauge chosen for our calculation, all the squared diagrams and interference terms that involve a 4-gluon vertex are identically zero. The corresponding  $D_i$ s are given in Table 10 of Appendix A. Using the combinations from Eqs. (4.33)-(4.35) and then the definition from Eq. (4.55) leads to the following set of the off-shell hard factors

$$K_{gg^* \rightarrow gg}^{(1)} = \frac{2N_c}{C_F} \frac{(\bar{s}^2 - \bar{t}\bar{u})^2}{\bar{t}\hat{t}\hat{u}\hat{u}\bar{s}\hat{s}} [\bar{u}\hat{u} + \bar{t}\hat{t}] , \quad (5.11)$$

$$K_{gg^* \rightarrow gg}^{(2)} = -\frac{N_c}{C_F} \frac{(\bar{s}^2 - \bar{t}\bar{u})^2}{\bar{t}\hat{t}\hat{u}\hat{u}\bar{s}\hat{s}} [\bar{u}\hat{u} + \bar{t}\hat{t} - \bar{s}\hat{s}] . \quad (5.12)$$

The on-shell limit is again manifest, with the above equations reducing to those from Table 1 as  $|k_t| \rightarrow 0$ .

## 6 Helicity method for TMD amplitudes

In the preceding sections, the hard factors accompanying the gluon densities  $\mathcal{F}_{ag}^{(i)}$  were calculated from the squared diagrams presented in Figs. 3-6. This procedure has certain drawbacks, especially when one would like to consider more complicated processes. For multiparticle processes, the color decompositions and helicity method [26, 49] are now considered as the most effective ways to deal with them. Moreover, it is not obvious how the gauge invariance comes into play for the separate diagrams from Figs. 3-6 contributing to the hard factors. In the color decomposition method, the so-called *color ordered amplitudes* are gauge invariant from the start and one can use them directly to construct hard factors.

In view of the above, and to cross-check the results from Section 5, we will give an alternative procedure to obtain the factorization formulas with off-shell gluon. To this end, we shall need TMD gluon densities corresponding to color decomposition of amplitudes and the color-ordered amplitudes themselves.

### 6.1 Color decompositions

Let us recall some basic facts about the color decompositions. We refer to [26, 49] for more details.

We first consider a gluon amplitude  $\mathcal{M}^{a_1 \dots a_N}(\varepsilon_1^{\lambda_1}, \dots, \varepsilon_N^{\lambda_N})$ , where  $a_1, \dots, a_N$  are the external, adjoint color quantum numbers, the  $\varepsilon_i^{\lambda_i}$  is a polarization vector for a gluon  $i$  having momentum  $k_i$  and helicity  $\lambda_i = \pm$ . The fundamental color decomposition reads

$$\mathcal{M}^{a_1 \dots a_N}(\varepsilon_1^{\lambda_1}, \dots, \varepsilon_N^{\lambda_N}) = \sum_{\sigma \in S_{N-1}} \text{Tr}(t^{a_1} t^{a_{\sigma_2}} \dots t^{a_{\sigma_N}}) \mathcal{M}(1^{\lambda_1}, \sigma_2^{\lambda_{\sigma_2}} \dots, \sigma_N^{\lambda_{\sigma_N}}) , \quad (6.1)$$



where the sum is over a set  $S_{N-1}$  of all non-cyclic permutations of  $\{1, \dots, N\}$ . The coefficients of the expansion define color ordered – or dual – amplitudes. They possess several useful properties. First of all, they are gauge invariant. Second, there are certain relations between dual amplitudes. Indeed, the following adjoint color decomposition involves only  $(N-2)!$  different amplitudes [50]

$$\mathcal{M}^{a_1 \dots a_N} \left( \varepsilon_1^{\lambda_1}, \dots, \varepsilon_N^{\lambda_N} \right) = \sum_{\sigma \in S_{N-2}} (F^{a_{\sigma_2}} \dots F^{a_{\sigma_{N-1}}})_{a_1 a_N} \mathcal{M} \left( 1^{\lambda_1}, \sigma_2^{\lambda_{\sigma_2}}, \dots, \sigma_{N-1}^{\lambda_{\sigma_{N-1}}}, N^{\lambda_N} \right), \quad (6.2)$$

where  $(F^a)_{bc} = f_{abc}$ .

Consider now an amplitude involving a quark anti-quark pair  $\mathcal{M}^{D_1 a_2 \dots a_{N-1} \bar{D}_N}$  where  $D_i, \bar{D}_j$  are the color and the anti-color of the quark and the anti-quark, respectively. The color decomposition reads

$$\mathcal{M}^{D_1 a_2 \dots a_{N-1} \bar{D}_N} \left( \lambda_1, \varepsilon_2^{\lambda_2}, \dots, \varepsilon_{N-1}^{\lambda_{N-1}}, \lambda_N \right) = \sum_{\sigma \in S_{N-2}} (t^{a_{\sigma_2}} \dots t^{a_{\sigma_{N-1}}})_{D_1 \bar{D}_N} \mathcal{M} \left( 1^{\lambda_1}, \sigma_2^{\lambda_{\sigma_2}}, \dots, \sigma_{N-1}^{\lambda_{\sigma_{N-1}}}, N^{\lambda_N} \right). \quad (6.3)$$

Now  $\lambda_1$  and  $\lambda_N$  are helicities of the quark and the anti-quark. For amplitudes involving more quark anti-quark pairs the decomposition is more complicated and we refer to [26] for details.

It is important to note that the above color decompositions work also for the case when one of the gluons is off-shell.

## 6.2 Gluon TMDs for color ordered amplitudes

Let us now find the gluon TMDs corresponding to the color ordered amplitudes squared, as defined in the previous subsection. We constraint ourselves to the  $2 \rightarrow 2$  processes case considered in this paper.

Let us first consider the  $g(k_4) g^*(k_1) \rightarrow g(k_3) g(k_2)$  process. For the purpose of this and next subsections we have assigned a new set of momenta to the partons. This assignment differs from the one used before but it is more convenient when dealing with color ordered amplitudes. The correspondence is achieved by the following relations:  $k_1 \leftrightarrow k, k_2 \leftrightarrow p_1, k_3 \leftrightarrow p_2, k_4 \leftrightarrow p$ . Moreover, for the off-shell momentum we adopt a notation

$$k_1 = n_1 + k_T. \quad (6.4)$$

The color decomposition of the four gluon amplitude reads

$$\begin{aligned} \mathcal{M}_{gg^* \rightarrow gg}^{a_1 a_2 a_3 a_4} \left( n_1, \varepsilon_2^{\lambda_2}, \varepsilon_3^{\lambda_3}, \varepsilon_4^{\lambda_4} \right) &= f_{a_1 a_2 c} f_{c a_3 a_4} \mathcal{M}_{gg^* \rightarrow gg} \left( 1^*, 2^{\lambda_2}, 3^{\lambda_3}, 4^{\lambda_4} \right) \\ &+ f_{a_1 a_3 c} f_{c a_2 a_4} \mathcal{M}_{gg^* \rightarrow gg} \left( 1^*, 3^{\lambda_3}, 2^{\lambda_2}, 4^{\lambda_4} \right), \end{aligned} \quad (6.5)$$

where  $n_1$  is placed for the off-shell gluon instead of a polarization vector (in fact it plays a similar role). As far as dual amplitudes are concerned, we indicate the off-shell gluon by a star. In Table 4. we calculate the gluon TMDs that correspond to the color structures exposed in (6.5) (after squaring). They agree with the gluon TMDs calculated in [12] and listed in rows 1 and 3 of Table 8 of [12]. That table defines one more gluon TMD (the row 2) which however is redundant. Clearly, the color decomposition (6.5) gives all the necessary color structures and already incorporates the gauge invariance. In summary, the two gluon TMD listed in Table 4

color-ordered amplitude squared	gluon TMD
$ \mathcal{M}_{gg^* \rightarrow gg}(1^*, 2^{\lambda_2}, 3^{\lambda_3}, 4^{\lambda_4}) ^2$ $ \mathcal{M}_{gg^* \rightarrow gg}(1^*, 3^{\lambda_3}, 2^{\lambda_2}, 4^{\lambda_4}) ^2$	$\Phi_{gg \rightarrow gg}^{(1)} = \frac{1}{2N_c^2} (N_c^2 \mathcal{F}_{gg}^{(1)} - 2\mathcal{F}_{gg}^{(3)})$ $+ \mathcal{F}_{gg}^{(4)} + \mathcal{F}_{gg}^{(5)} + N_c^2 \mathcal{F}_{gg}^{(6)}$
$\mathcal{M}_{gg^* \rightarrow gg}(1^*, 2^{\lambda_2}, 3^{\lambda_3}, 4^{\lambda_4}) \mathcal{M}_{gg^* \rightarrow gg}^*(1^*, 3^{\lambda_3}, 2^{\lambda_2}, 4^{\lambda_4})$ $\mathcal{M}_{gg^* \rightarrow gg}^*(1^*, 2^{\lambda_2}, 3^{\lambda_3}, 4^{\lambda_4}) \mathcal{M}_{gg^* \rightarrow gg}(1^*, 3^{\lambda_3}, 2^{\lambda_2}, 4^{\lambda_4})$	$\Phi_{gg \rightarrow gg}^{(2)} = \frac{1}{N_c^2} (N_c^2 \mathcal{F}_{gg}^{(2)} - 2\mathcal{F}_{gg}^{(3)})$ $+ \mathcal{F}_{gg}^{(4)} + \mathcal{F}_{gg}^{(5)} + N_c^2 \mathcal{F}_{gg}^{(6)}$

Table 4: Gluon TMDs accompanying the color-ordered amplitudes for  $gg^* \rightarrow gg$  process. It has been assumed that TMDs are real. The  $\mathcal{F}_{gg}^{(i)}$  distributions are defined in Eqs. (4.15), (4.16), (4.17) and in Eqs. (4.30), (4.31), (4.32).

color-ordered amplitude squared	gluon TMD
$ \mathcal{M}_{gg^* \rightarrow q\bar{q}}(2^{\lambda_2}, 1^*, 4^{\lambda_4}, 3^{\lambda_3}) ^2$ $ \mathcal{M}_{gg^* \rightarrow q\bar{q}}(2^{\lambda_2}, 4^{\lambda_4}, 1^*, 3^{\lambda_3}) ^2$	$\Phi_{gg \rightarrow q\bar{q}}^{(1)} = \frac{1}{N_c^2 - 1} (N_c^2 \mathcal{F}_{gg}^{(1)} - \mathcal{F}_{gg}^{(3)})$
$\mathcal{M}_{gg^* \rightarrow q\bar{q}}(2^{\lambda_2}, 1^*, 4^{\lambda_4}, 3^{\lambda_3}) \mathcal{M}_{gg^* \rightarrow q\bar{q}}^*(2^{\lambda_2}, 4^{\lambda_4}, 1^*, 3^{\lambda_3})$ $\mathcal{M}_{gg^* \rightarrow q\bar{q}}^*(2^{\lambda_2}, 1^*, 4^{\lambda_4}, 3^{\lambda_3}) \mathcal{M}_{gg^* \rightarrow q\bar{q}}(2^{\lambda_2}, 4^{\lambda_4}, 1^*, 3^{\lambda_3})$	$\Phi_{gg \rightarrow q\bar{q}}^{(2)} = -N_c^2 \mathcal{F}_{gg}^{(2)} + \mathcal{F}_{gg}^{(3)}$

Table 5: Gluon TMDs accompanying the color-ordered amplitudes for  $gg^* \rightarrow q\bar{q}$  process. It has been assumed that correlators are real. The  $\mathcal{F}_{gg}^{(i)}$  distributions are defined in Eqs. (4.15), (4.16) and (4.17).

are the only relevant TMDs and correspond to the two independent gauge invariant amplitudes squared and their interference.

Now, let us turn to the  $g(k_4) g^*(k_1) \rightarrow \bar{q}(k_3) q(k_2)$  process. The color decomposition reads

$$\begin{aligned} \mathcal{M}_{gg^* \rightarrow q\bar{q}}^{D_2 a_1 a_4 \bar{D}_3}(\lambda_2, n_1, \varepsilon_4^{\lambda_4}, \lambda_3) &= (t^{a_1} t^{a_4})_{D_2 \bar{D}_3} \mathcal{M}_{gg^* \rightarrow q\bar{q}}(2^{\lambda_2}, 1^*, 4^{\lambda_4}, 3^{\lambda_3}) \\ &+ (t^{a_4} t^{a_1})_{D_2 \bar{D}_3} \mathcal{M}_{gg^* \rightarrow q\bar{q}}(2^{\lambda_2}, 4^{\lambda_4}, 1^*, 3^{\lambda_3}). \end{aligned} \quad (6.6)$$

The gluon TMDs corresponding to the color structures appearing after squaring this equation are gathered in Table 5. They correspond to rows 1 and 5 of Table 7 in [12]. Again, we have only two independent TMDs that are needed.

For the process  $q(k_4) g^*(k_1) \rightarrow q(k_3) g(k_2)$ , the color decomposition reads

$$\begin{aligned} \mathcal{M}_{qg^* \rightarrow qg}^{D_3 a_1 a_2 \bar{D}_4}(\lambda_3, n_1, \varepsilon_2^{\lambda_2}, \lambda_4) &= (t^{a_1} t^{a_2})_{D_3 \bar{D}_4} \mathcal{M}_{qg^* \rightarrow qg}(3^{\lambda_3}, 1^*, 2^{\lambda_2}, 4^{\lambda_4}) + \\ &(t^{a_2} t^{a_1})_{D_3 \bar{D}_4} \mathcal{M}_{qg^* \rightarrow qg}(3^{\lambda_3}, 2^{\lambda_2}, 1^*, 4^{\lambda_4}). \end{aligned} \quad (6.7)$$

For anti-quarks we need to exchange the indices  $3 \leftrightarrow 4$ . The TMDs corresponding to those processes are given in Table 6. In general, the TMDs for a sub-process with anti-quarks are

color-ordered amplitude squared	gluon TMD
$\mathcal{M}_{qg^* \rightarrow qg} (3^{\lambda_3}, 1^*, 2^{\lambda_2}, 4^{\lambda_4}) \mathcal{M}_{qg^* \rightarrow qg}^* (3^{\lambda_3}, 2^{\lambda_2}, 1^*, 4^{\lambda_4})$ $\mathcal{M}_{qg^* \rightarrow qg}^* (3^{\lambda_3}, 1^*, 2^{\lambda_2}, \lambda_4) \mathcal{M}_{qg^* \rightarrow qg} (3^{\lambda_3}, 2^{\lambda_2}, 1^*, 4^{\lambda_4})$ $ \mathcal{M}_{qg^* \rightarrow qg} (3^{\lambda_3}, 2^{\lambda_2}, 1^*, 4^{\lambda_4}) ^2$	$\Phi_{qg \rightarrow qg}^{(1)} = \mathcal{F}_{qg}^{(1)}$
$ \mathcal{M}_{qg^* \rightarrow qg} (3^{\lambda_3}, 1^*, 2^{\lambda_2}, 4^{\lambda_4}) ^2$	$\Phi_{qg \rightarrow qg}^{(2)} = \frac{1}{N_c^2 - 1} \left( -\mathcal{F}_{qg}^{(1)} + N_c^2 \mathcal{F}_{qg}^{(2)} \right)$

Table 6: Gluon TMDs accompanying the color-ordered amplitudes for  $qg^* \rightarrow qg$  process. It has been assumed that correlators are real. The  $\mathcal{F}_{qg}^{(i)}$  distributions are defined in Eqs. (4.4) and Eqs. (4.5).

different than for quarks, but they turn out to be the same assuming that the correlators are real. Again, we end up with only two independent TMDs.

### 6.3 Off-shell color-ordered helicity amplitudes

In Section 5, we have calculated the off-shell hard factors in a specific axial gauge, with  $p_A$  chosen as the gauge vector, and using the high energy projector (5.1). As shown in Ref. [10], such a procedure yields results which are gauge invariant within a subclass of axial gauges with the gauge vector  $n^\mu = ap_p^\mu + bp_A^\mu$ , where  $a$  and  $b$  are arbitrary complex numbers. There are also methods to calculate gauge invariant off-shell amplitudes in any gauge and choice of polarization vectors [34, 35, 47, 48]. In what follows, we shall use those methods and specifically the results of [35, 48].

Consider first the gluon amplitudes. For the purpose of this section only we assume all momenta to be outgoing. For the non-vanishing helicity configurations, in the helicity basis, we have

$$\mathcal{M}_{g^*g \rightarrow gg} (1^*, 2^-, 3^+, 4^+) = 2g^2 \rho_1 \frac{\langle 1^*2 \rangle^4}{\langle 1^*2 \rangle \langle 23 \rangle \langle 34 \rangle \langle 41^* \rangle}, \quad (6.8)$$

$$\mathcal{M}_{g^*g \rightarrow gg} (1^*, 2^+, 3^-, 4^+) = 2g^2 \rho_1 \frac{\langle 1^*3 \rangle^4}{\langle 1^*2 \rangle \langle 23 \rangle \langle 34 \rangle \langle 41^* \rangle}, \quad (6.9)$$

$$\mathcal{M}_{g^*g \rightarrow gg} (1^*, 2^+, 3^+, 4^-) = 2g^2 \rho_1 \frac{\langle 1^*4 \rangle^4}{\langle 1^*2 \rangle \langle 23 \rangle \langle 34 \rangle \langle 41^* \rangle}, \quad (6.10)$$

where we adopted a shorthand notation for the spinor products  $\langle ij \rangle = \langle k_i - |k_j \rangle$  with  $|k_i \pm \rangle = \frac{1}{2} (1 \pm \gamma_5) u(k_i)$ , and where  $\rho_1$  is a, for our purposes irrelevant, phase factor (see details *e.g.* in [48]). We also defined  $\langle 1^*i \rangle = \langle n_1 i \rangle$  with  $n_1$  being the longitudinal component of  $k_1$ , *c.f.* Eq. (6.4). The other remaining helicity configurations can be obtained from Eqs. (6.8)-(6.10) using CP invariance

$$\mathcal{M}_{gg^* \rightarrow gg} (1^*, 2^+, 3^-, 4^-) = \mathcal{M}_{gg^* \rightarrow gg}^* (1^*, 2^-, 3^+, 4^+), \quad (6.11)$$

and so on. For the other color ordered amplitude,  $\mathcal{M}_{gg^* \rightarrow gg} (1^*, 3, 2, 4)$ , we need to exchange  $2 \leftrightarrow 3$  in the denominators.

The above helicity amplitudes can be efficiently evaluated and squared numerically, however for the purpose of this paper we shall need analytic expressions. To this end let us introduce

$[ij] = \langle k_i + |k_j - \rangle$ , which, up to an unimportant phase, is a complex conjugate of  $\langle ij \rangle$ . Moreover, we have the following relation

$$\langle ij \rangle [ji] = (k_i + k_j)^2 \equiv \tilde{s}_{ij}. \quad (6.12)$$

For the products involving  $n_1$  we use the notation

$$\langle 1^* i \rangle [i 1^*] = (n_1 + k_i)^2 \equiv \tilde{s}_{1^* i}. \quad (6.13)$$

With this, we get for the required amplitudes squared summed and averaged over helicities

$$|\overline{\mathcal{M}}_{gg^* \rightarrow gg}(1^*, 2, 3, 4)|^2 = 8g^4 \frac{\tilde{s}_{1^* 2}^4 + \tilde{s}_{1^* 3}^4 + \tilde{s}_{1^* 4}^4}{\tilde{s}_{1^* 2} \tilde{s}_{23} \tilde{s}_{34} \tilde{s}_{41^*}}, \quad (6.14)$$

$$|\overline{\mathcal{M}}_{gg^* \rightarrow gg}(1^*, 3, 2, 4)|^2 = 8g^4 \frac{\tilde{s}_{1^* 2}^4 + \tilde{s}_{1^* 3}^4 + \tilde{s}_{1^* 4}^4}{\tilde{s}_{1^* 3} \tilde{s}_{32} \tilde{s}_{24} \tilde{s}_{41^*}}, \quad (6.15)$$

$$\overline{\mathcal{M}}_{gg^* \rightarrow gg}(1^*, 2, 3, 4) \overline{\mathcal{M}}_{gg^* \rightarrow gg}^*(1^*, 3, 2, 4) = -8g^4 \frac{\tilde{s}_{1^* 2}^4 + \tilde{s}_{1^* 3}^4 + \tilde{s}_{1^* 4}^4}{\langle 1^* 2 \rangle \langle 34 \rangle [1^* 3] [24] \tilde{s}_{23} \tilde{s}_{41^*}}, \quad (6.16)$$

$$\overline{\mathcal{M}}_{gg^* \rightarrow gg}^*(1^*, 2, 3, 4) \overline{\mathcal{M}}_{gg^* \rightarrow gg}(1^*, 3, 2, 4) = -8g^4 \frac{\tilde{s}_{1^* 2}^4 + \tilde{s}_{1^* 3}^4 + \tilde{s}_{1^* 4}^4}{[1^* 2] [34] \langle 1^* 3 \rangle \langle 24 \rangle \tilde{s}_{23} \tilde{s}_{41^*}}, \quad (6.17)$$

where we have used overlines to indicate helicity summations. The last two interference terms enter the cross section as a sum. Therefore, we may simplify it as

$$\begin{aligned} & \overline{\mathcal{M}}_{gg^* \rightarrow gg}(1^*, 2, 3, 4) \overline{\mathcal{M}}_{gg^* \rightarrow gg}^*(1^*, 3, 2, 4) + \overline{\mathcal{M}}_{gg^* \rightarrow gg}^*(1^*, 2, 3, 4) \overline{\mathcal{M}}_{gg^* \rightarrow gg}(1^*, 3, 2, 4) \\ &= -8g^4 \frac{(\tilde{s}_{1^* 2}^4 + \tilde{s}_{1^* 3}^4 + \tilde{s}_{1^* 4}^4)(\tilde{s}_{24} \tilde{s}_{1^* 3} - \tilde{s}_{23} \tilde{s}_{1^* 4} + \tilde{s}_{34} \tilde{s}_{1^* 2})}{\tilde{s}_{1^* 2} \tilde{s}_{34} \tilde{s}_{1^* 3} \tilde{s}_{24} \tilde{s}_{23} \tilde{s}_{41^*}}, \end{aligned} \quad (6.18)$$

where we have used

$$[1^* 2] [34] \langle 1^* 3 \rangle \langle 24 \rangle + \langle 1^* 2 \rangle \langle 34 \rangle [1^* 3] [24] = \langle n_1 - |\not{p}_3 \not{p}_4 \not{p}_2 | n_1 - \rangle + \langle n_1 - |\not{p}_2 \not{p}_4 \not{p}_3 | n_1 - \rangle, \quad (6.19)$$

and applied  $\not{p}_i \not{p}_j = \tilde{s}_{ij} - \not{p}_j \not{p}_i$  a few times. The amplitudes for the on-shell limit are simply obtained by dropping the star in  $1^*$  so that the spinor and the scalar products will be with  $k_1$  instead of  $n_1$ .

Now let us turn to processes with quarks. We will give only amplitudes for  $g(k_4) g^*(k_1) \rightarrow \bar{q}(k_3) q(k_2)$  process, as all the other can be obtained by the crossing symmetry (taking care of the proper color flow when crossing). We have

$$\mathcal{M}_{gg^* \rightarrow q\bar{q}}(3^-, 1^*, 4^+, 2^+) = 2g^2 \rho_1 \frac{\langle 21^* \rangle^3 \langle 31^* \rangle}{\langle 21^* \rangle \langle 1^* 4 \rangle \langle 43 \rangle \langle 32 \rangle}, \quad (6.20)$$

$$\mathcal{M}_{gg^* \rightarrow q\bar{q}}(3^+, 1^*, 4^+, 2^-) = 2g^2 \rho_1 \frac{\langle 31^* \rangle^3 \langle 21^* \rangle}{\langle 21^* \rangle \langle 1^* 4 \rangle \langle 43 \rangle \langle 32 \rangle}. \quad (6.21)$$

We note that the above formulas have never been published in the literature and are given here for the first time.

Similar as before, the two remaining helicity configurations can be obtained thanks to CP symmetry. For the color ordered amplitudes with 1 and 4 interchanged, we need to make a replacement  $1 \leftrightarrow 4$  in the denominators. The amplitudes squared and summed over helicities

read (the helicity averaging factor is included)

$$|\overline{\mathcal{M}}_{gg^* \rightarrow q\bar{q}}(3, 1^*, 4, 2)|^2 = 2g^4 \frac{\tilde{s}_{1^*3}(\tilde{s}_{1^*2}^2 + \tilde{s}_{1^*3}^2)}{\tilde{s}_{1^*4}\tilde{s}_{34}\tilde{s}_{23}}, \quad (6.22)$$

$$|\overline{\mathcal{M}}_{gg^* \rightarrow q\bar{q}}(3, 4, 1^*, 2)|^2 = 2g^4 \frac{\tilde{s}_{1^*2}(\tilde{s}_{1^*2}^2 + \tilde{s}_{1^*3}^2)}{\tilde{s}_{1^*4}\tilde{s}_{24}\tilde{s}_{23}}, \quad (6.23)$$

$$\overline{\mathcal{M}}_{gg^* \rightarrow q\bar{q}}(3, 1^*, 4, 2) \overline{\mathcal{M}}_{gg^* \rightarrow q\bar{q}}^*(3, 4, 1^*, 2) = -2g^4 \frac{\tilde{s}_{1^*2}\tilde{s}_{1^*3}(\tilde{s}_{1^*2}^2 + \tilde{s}_{1^*3}^2)}{\langle 21^* \rangle \langle 43 \rangle [31^*] [42] \tilde{s}_{23} \tilde{s}_{41^*}}, \quad (6.24)$$

$$\overline{\mathcal{M}}_{gg^* \rightarrow q\bar{q}}^*(3, 1^*, 4, 2) \overline{\mathcal{M}}_{gg^* \rightarrow q\bar{q}}(3, 4, 1^*, 2) = -2g^4 \frac{\tilde{s}_{1^*2}\tilde{s}_{1^*3}(\tilde{s}_{1^*2}^2 + \tilde{s}_{1^*3}^2)}{[21^*] [43] \langle 31^* \rangle \langle 42 \rangle \tilde{s}_{23} \tilde{s}_{41^*}}. \quad (6.25)$$

The sum of the last two interference terms simplifies to

$$\begin{aligned} & \overline{\mathcal{M}}_{gg^* \rightarrow q\bar{q}}(3, 1^*, 4, 2) \overline{\mathcal{M}}_{gg^* \rightarrow q\bar{q}}^*(3, 4, 1^*, 2) + \overline{\mathcal{M}}_{gg^* \rightarrow q\bar{q}}^*(3, 1^*, 4, 2) \overline{\mathcal{M}}_{gg^* \rightarrow q\bar{q}}(3, 4, 1^*, 2) \\ &= -2g^4 \frac{\tilde{s}_{1^*2}\tilde{s}_{1^*3}(\tilde{s}_{1^*2}^2 + \tilde{s}_{1^*3}^2)(\tilde{s}_{24}\tilde{s}_{1^*3} - \tilde{s}_{23}\tilde{s}_{1^*4} + \tilde{s}_{34}\tilde{s}_{1^*2})}{\tilde{s}_{1^*2}\tilde{s}_{34}\tilde{s}_{1^*3}\tilde{s}_{24}\tilde{s}_{23}\tilde{s}_{41^*}}. \end{aligned} \quad (6.26)$$

In order to obtain amplitudes for  $q(k_4) g^*(k_1) \rightarrow q(k_3) g(k_2)$  we can use the crossing symmetry. Specifically, we can obtain  $|\overline{\mathcal{M}}_{gg^* \rightarrow qg}(3, 1^*, 2, 4)|^2$ ,  $|\overline{\mathcal{M}}_{gg^* \rightarrow qg}(3, 2, 1^*, 4)|^2$  and interference terms by making replacement  $2 \leftrightarrow 4$  in Eqs. (6.23), (6.22), (6.26) respectively.

## 6.4 Hard factors from color-ordered amplitudes

Having computed the color ordered amplitudes it is now straightforward to calculate the hard factors  $K^{(i)}$ . Let us note, that it is the  $K^{(i)}$  hard factors that appear naturally within the color-ordered formalism, not the  $H^{(i)}$  factors. It also comes naturally that there are two hard factors and two TMDs per each channel, so the factorization formulas can be written in a unified form:

$$\frac{d\sigma^{pA \rightarrow \text{dijets}+X}}{d^2P_t d^2k_t dy_1 dy_2} = \frac{\alpha_s^2}{(x_1 x_2 s)^2} \sum_{a,c,d} x_1 f_{a/p}(x_1, \mu^2) \sum_{i=1}^2 K_{ag^* \rightarrow cd}^{(i)} \Phi_{ag \rightarrow cd}^{(i)} \frac{1}{1 + \delta_{cd}}, \quad (6.27)$$

where  $a, c, d$  are the contributing partons. The explicit expressions for the generalized gluon TMDs  $\Phi_{ag \rightarrow cd}^{(i)}$  are listed in Tables 4-6. The hard factors  $K^i$  were already given in Section 5 (we collect them in Table 7 for convenience). In the context of this section, they are obtained by multiplying the left column of Tables 4-6 by the corresponding color factors and combining the cells that belong to the same generalized TMD. More precisely, we have

$$g^4 K_{gg^* \rightarrow gg}^{(1)} = \frac{1}{(2N_c C_F)^2} \frac{N_c^3 C_F}{2} \left( |\overline{\mathcal{M}}_{gg^* \rightarrow gg}(1^*, 2, 3, 4)|^2 + |\overline{\mathcal{M}}_{gg^* \rightarrow gg}(1^*, 3, 2, 4)|^2 \right), \quad (6.28)$$

$$g^4 K_{gg^* \rightarrow gg}^{(2)} = \frac{1}{(2N_c C_F)^2} \frac{N_c^3 C_F}{4} \left( \overline{\mathcal{M}}_{gg^* \rightarrow gg}(1^*, 2, 3, 4) \overline{\mathcal{M}}_{gg^* \rightarrow gg}^*(1^*, 3, 2, 4) + \text{c.c.} \right), \quad (6.29)$$

for pure gluon channel, and

$$g^4 K_{gg^* \rightarrow q\bar{q}}^{(1)} = \frac{1}{(2N_c C_F)^2} N_c C_F^2 \left( |\overline{\mathcal{M}}_{gg^* \rightarrow q\bar{q}}(3, 1^*, 4, 2)|^2 + |\overline{\mathcal{M}}_{gg^* \rightarrow q\bar{q}}(3, 4, 1^*, 2)|^2 \right), \quad (6.30)$$

$$g^4 K_{gg^* \rightarrow q\bar{q}}^{(2)} = \frac{1}{(2N_c C_F)^2} \frac{-C_F}{2} \left( \overline{\mathcal{M}}_{gg^* \rightarrow q\bar{q}}(3, 1^*, 4, 2) \overline{\mathcal{M}}_{gg^* \rightarrow q\bar{q}}^*(3, 4, 1^*, 2) + \text{c.c.} \right), \quad (6.31)$$

$i$	1	2
$K_{gg^* \rightarrow gg}^{(i)}$	$\frac{N_c}{C_F} \frac{(\bar{s}^4 + \bar{t}^4 + \bar{u}^4) (\bar{u}\hat{u} + \bar{t}\hat{t})}{\hat{t}\hat{t}\hat{u}\hat{u}\hat{s}\hat{s}}$	$-\frac{N_c}{2C_F} \frac{(\bar{s}^4 + \bar{t}^4 + \bar{u}^4) (\bar{u}\hat{u} + \bar{t}\hat{t} - \bar{s}\hat{s})}{\hat{t}\hat{t}\hat{u}\hat{u}\hat{s}\hat{s}}$
$K_{gg^* \rightarrow q\bar{q}}^{(i)}$	$\frac{1}{2N_c} \frac{(\bar{t}^2 + \bar{u}^2) (\bar{u}\hat{u} + \bar{t}\hat{t})}{\bar{s}\hat{s}\hat{t}\hat{u}}$	$\frac{1}{4N_c^2 C_F} \frac{(\bar{t}^2 + \bar{u}^2) (\bar{u}\hat{u} + \bar{t}\hat{t} - \bar{s}\hat{s})}{\bar{s}\hat{s}\hat{t}\hat{u}}$
$K_{qg^* \rightarrow qg}^{(i)}$	$-\frac{\bar{u}(\bar{s}^2 + \bar{u}^2)}{2\hat{t}\hat{t}\hat{s}} \left(1 + \frac{\bar{s}\hat{s} - \bar{t}\hat{t}}{N_c^2 \bar{u}\hat{u}}\right)$	$-\frac{C_F}{N_c} \frac{\bar{s}(\bar{s}^2 + \bar{u}^2)}{\hat{t}\hat{t}\hat{u}}$

Table 7: The hard factors accompanying the gluon TMDs  $\Phi_{ag \rightarrow cd}^{(i)}$ .

for  $gg^* \rightarrow q\bar{q}$  channel. For the  $qg^* \rightarrow qg$  sub-process we need to use the crossing symmetry as described in the preceding section. We have

$$g^4 K_{qg^* \rightarrow qg}^{(1)} = \frac{1}{2C_F N_c^2} \left\{ N_c C_F^2 \left( -|\overline{\mathcal{M}}_{gg^* \rightarrow q\bar{q}}(3, 1^*, 4, 2)|^2 \right)_{2 \leftrightarrow 4} - \frac{C_F}{2} \left( -\overline{\mathcal{M}}_{gg^* \rightarrow q\bar{q}}(3, 1^*, 4, 2) \overline{\mathcal{M}}_{gg^* \rightarrow q\bar{q}}^*(3, 4, 1^*, 2) - \text{c.c.} \right)_{2 \leftrightarrow 4} \right\}, \quad (6.32)$$

$$g^4 K_{qg^* \rightarrow qg}^{(2)} = \frac{1}{2C_F N_c^2} N_c C_F^2 \left( -|\overline{\mathcal{M}}_{gg^* \rightarrow q\bar{q}}(3, 4, 1^*, 2)|^2 \right)_{2 \leftrightarrow 4}. \quad (6.33)$$

In all the formulas above, the first color factor comes from color averaging. The minus signs in front of the amplitudes in (6.32), (6.33) come from the crossing of a fermion line. Table 7 is easily recovered using the following relations of  $\tilde{s}_{ij}$  to the kinematic variables from Section 5

$$\tilde{s}_{23} = \tilde{s}_{14} = \hat{s}, \quad \tilde{s}_{34} = \tilde{s}_{12} = \hat{t}, \quad \tilde{s}_{24} = \tilde{s}_{13} = \hat{u}, \quad (6.34)$$

$$\tilde{s}_{1^*4} = \bar{s}, \quad \tilde{s}_{1^*2} = \bar{t}, \quad \tilde{s}_{1^*3} = \bar{u}. \quad (6.35)$$

## 7 Conclusions and outlook

Dijet production is one of the key processes studied at the LHC. Requiring the two jets to be produced in the forward direction creates an asymmetric situation, in which one of the incoming hadrons is probed at large  $x$ , while the other is probed at a very small momentum fraction. This kinematic regime poses various challenges, one of the biggest questions being the existence of a theoretically-consistent and, at the same time, practically-manageable factorization formula. The standard collinear factorization is not applicable in this case as the dependence on the transverse momentum of the low- $x$  gluon in the target,  $k_t$ , cannot be neglected.

In the limit where the jets' transverse momenta  $|p_{1t}|, |p_{2t}| \gg |k_t| \sim Q_s$ , with the latter being the saturation scale of the target, an effective transverse-momentum-dependent factorization formula for forward dijet production has been derived in Refs. [13, 14] and it has been shown to be consistent with the CGC framework. On the other side, the high energy factorization approach [10, 11] has been also successfully applied for studying forward dijet production at the LHC. In this paper, we have examined the theoretical status of the HEF approach in the context of forward dijet production at hadron colliders and reconciled it with the TMD factorization by

creating a unified framework valid in the limit  $|p_{1t}|, |p_{2t}| \gg Q_s$  with an arbitrary value of  $|k_t|$ , as long as it is allowed by phase space constraints. In particular, we have shown in Section 3 that the HEF formula is indeed justified in the kinematic window of  $|p_{1t}|, |p_{2t}| \sim |k_t| \gg Q_s$ , where it was explicitly derived from CGC for all  $2 \rightarrow 2$  channels. This limit corresponds to the dilute target approximation hence no non-linear effects are expected.

The second major result of our work is an improvement of the effective TMD factorization for forward dijet production, first derived in Ref. [13], by taking into account in Section 4 all finite- $N_c$  corrections, as well as generalizing the factorization formula to the case with an off-shell incoming gluon in Sections 5 and 6. In addition, we were able to simplify the TMD factorization formula by reducing the number of gluon distributions to two independent TMDs for each channel. The main results of this part of our study are summarized in Eq. (6.27), which gives the new TMD factorization formula, as well as in Table 7, where we collect all the off-shell hard factors. The corresponding gluon distributions are given in Tables 4, 5 and 6. The above results were obtained with two independent techniques: a traditional Feynman diagram approach and helicity methods with color ordered amplitudes. The improved TMD factorization formula (6.27) encapsulates both the result of Ref. [13] and the HEF framework as its limiting cases.

The results obtained in this paper open several avenues for future research that we plan to follow. First, a natural next steps will be to use Eq. (6.27) for phenomenological studies. That shall require some input for the six gluon TMDs  $\Phi_{ag \rightarrow cd}^{(1,2)}(x, k_t)$ , which may be difficult in a general case. But in the large- $N_c$  limit, they can all be written in terms of just two functions:  $xG^{(1)}(x, k_t)$  and  $xG^{(2)}(x, k_t)$ , which in turn can be evaluated within certain models, as in [5].

Another line of possible extension of our framework is to supplement it with high- $|P_t|$  effects such as Sudakov logarithms or coherence in the evolution of the gluon density. Essentially, this can be done by adding a  $\mu^2$  dependence to the unintegrated gluon distributions [29–31, 51–54]. The equations that combine such effects with the small- $x$  evolution [55, 56] show a nontrivial interplay between the non-linearities and the  $\mu^2$  dependence and this may, in particular, weaken the saturation effects. At the linear level, the so-called single step inclusion of the hard-scale effects (as demonstrated in [17]) helps in the description of forward-central dijet data, therefore this direction seems to be relevant in order to provide complete predictions. Furthermore, first estimates of azimuthal decorrelations of the forward-forward dijets in the HEF framework, with inclusion of hard scale effects and non-linearities, show that they are of similar relevance for this process [33].

Last but not least, it remains to be proved that the large logarithms generated by higher-order corrections can indeed be absorbed into evolution equations for the various parton distributions (and jet fragmentation functions) involved, and potentially for additional soft factors [57]. This limitation however is not specific to our work, the same is true at the level of the TMD and HEF regimes independently. In the former case, it is known that TMD factorization generically does not apply for dijet production in hadron-hadron collisions [22, 24]. It is nevertheless expected that, in dilute-dense collisions, initial state interactions originating from a dilute hadron do not interfere with the intrinsic transverse momentum and thus factorization may hold, although there is no formal proof of this statement yet.

In addition, even though it was possible to write formula (4.56) in terms of just two TMDs per channel, this simplification may not survive after small- $x$  evolution is included, as, in general, the non-linear equations mix the original  $\mathcal{F}_{ag}^{(i)}$  functions. For instance,  $xG^{(1)}$  does not obey a closed equation and, contrary to what happens with  $xG^{(2)}$ , the large- $N_c$  limit does not help [58]. We note that any equivalent linear combination of the gluon distributions, such as (2.10) and (4.56), is equally valid, and it may turn out that some alternative choice allows one to write the evolution equations directly in terms of TMDs. By contrast, it is also possible that the inclusion

of small- $x$  evolution can only be achieved within the full complexity of the CGC, meaning that the  $Q_s \sim |k_t| \ll |P_t|$  limit, which allows one to avoid the quadrupole operator in (3.10) and express the cross section in terms of gluon distributions, may not help when small- $x$  evolution is considered.

In the HEF regime, the issues are different. The  $Q_s \ll |k_t| \sim |P_t|$  limit makes things simpler from the point of view of small- $x$  evolution, since non-linear effects can be neglected. However, the off-shellness of the hard process is not neglected and thus the standard power counting of the twist expansion becomes useless. One must then resort to different methods, such as those of Ref. [59]. Any progress towards an all-order proof of either HEF or TMD factorization for forward dijet production in dilute-dense collisions will naturally carry over to our improved TMD factorization formula (6.27) that combines both regimes. In the meantime, our results represent a viable alternative to CGC calculations, equivalent to them in the kinematic regime appropriate for dijets  $Q_s \ll |P_t|$  but more practical.

## Acknowledgments

The work of K.K. has been supported by Narodowe Centrum Nauki with Sonata Bis grant DEC-2013/10/E/ST2/00656. P.K. acknowledges the support of the grants DE-SC-0002145 and DE-FG02-93ER40771. S.S. acknowledges useful discussions with Gavin Salam and Fabrizio Caola. P.K., K.K., S.S. and A.vH. are grateful for hospitality to École Polytechnique, where part of this work has been carried out. K.K. thanks for the hospitality of Penn State University, where part of this research was done.

## A Off-shell expressions

In this appendix, we gather all expressions corresponding to the  $D_i$  diagrams from Fig. 3-6 in the case where one of the incoming gluons is off-shell. All calculations were performed in the axial gauge discussed at the beginning of Section 5, with the axial vectors for the on-shell gluons set according to Eq. (4.39).

For completeness, we also give here the results for the “old” hard factors defined in Eqs. (4.6), (4.7) (4.18), (4.19), (4.20), (4.33), (4.34) and (4.35), in the case with off-shell incoming gluon.

Table 8 gives the  $D_i$  expressions for the subprocesses  $qg^* \rightarrow qg$ . The two hard factors in this channel read

$$H_{qg^* \rightarrow qg}^{(1)} = -\frac{\bar{s}^2 + \bar{u}^2}{2\hat{s}\hat{t}\hat{u}} \left[ \bar{u} - \frac{\hat{t}\bar{t}}{N_c^2\hat{u}} \right], \quad (\text{A.1})$$

$$H_{qg^* \rightarrow qg}^{(2)} = -\frac{\bar{s}(\bar{s}^2 + \bar{u}^2)}{2\hat{u}\hat{t}\bar{t}}. \quad (\text{A.2})$$

In the limit,  $|k_t| \rightarrow 0$ , simplification given by Eq. (5.6) occurs and the above formulas manifestly recover the on-shell results from Eqs. (4.8) and (4.9).

The corresponding  $D_i$  results for the  $gg^* \rightarrow q\bar{q}$  subprocess are given in Table 9. The three



$qg^* \rightarrow qg$	$D_i$
(1)	$\frac{2\bar{t}\bar{u} + \bar{t}^2 + 2\bar{u}^2}{\hat{t}(\hat{s} + \hat{t} + \hat{u})}$
(2)	$\frac{C_F \bar{u} (2\bar{t}\bar{u} + \bar{t}^2 + 2\bar{u}^2)}{N_c \hat{u}\bar{t}(\hat{s} + \hat{t} + \hat{u})}$
(3)	$\frac{(2\bar{t}\bar{u} + \bar{t}^2 + 2\bar{u}^2) (\bar{t}(\hat{s} + \hat{t}) + \bar{u}(\hat{s} + \hat{u}))}{4\hat{t}\hat{u}\bar{t}(\hat{s} + \hat{t} + \hat{u})}$
(4)	$-\frac{C_F (\bar{t} + \bar{u}) (2\bar{t}\bar{u} + \bar{t}^2 + 2\bar{u}^2)}{N_c \hat{s}\bar{t}(\hat{s} + \hat{t} + \hat{u})}$
(5)	$-\frac{(2\bar{t}\bar{u} + \bar{t}^2 + 2\bar{u}^2) (\bar{t}(\hat{s} - \hat{t}) + \bar{u}(\hat{s} + \hat{u}))}{4\hat{s}\hat{t}\bar{t}(\hat{s} + \hat{t} + \hat{u})}$
(6)	$\frac{1}{N_c^2} \frac{(2\bar{t}\bar{u} + \bar{t}^2 + 2\bar{u}^2) (\bar{t}(\hat{s} + \hat{t}) + \bar{u}(\hat{s} - \hat{u}))}{4\hat{s}\hat{u}\bar{t}(\hat{s} + \hat{t} + \hat{u})}$

Table 8: Expressions for the  $qg^* \rightarrow qg$  subprocess with off-shell incoming gluon corresponding to diagrams (1)-(6) of Fig. 3 in gauge described in Section 5.

“old”, off-shell hard factors for this channel take the form

$$H_{gg^* \rightarrow q\bar{q}}^{(1)} = \frac{1}{4C_F} \frac{\bar{t}^2 + \bar{u}^2}{\hat{u}\hat{t}\hat{s}\bar{s}} [\hat{u}\bar{u} + \hat{t}\bar{t}] , \quad (\text{A.3})$$

$$H_{gg^* \rightarrow q\bar{q}}^{(2)} = \frac{1}{4C_F} \frac{\bar{t}^2 + \bar{u}^2}{\hat{u}\hat{t}\hat{s}\bar{s}} [\hat{s}\bar{s} - \hat{t}\bar{t} - \hat{u}\bar{u}] , \quad (\text{A.4})$$

$$H_{gg^* \rightarrow q\bar{q}}^{(3)} = -\frac{1}{4N_c^2 C_F} \frac{\bar{t}^2 + \bar{u}^2}{\hat{u}\hat{t}} . \quad (\text{A.5})$$

Again, following Eq. (5.6), it is manifest that the above hard factors reduce to Eqs. (4.21)-(4.23) in the limit  $|k_t| \rightarrow 0$ .

Finally, the  $D_i$  expressions for the subprocess  $gg^* \rightarrow gg$  are given in Table 10 and the six hard factors read

$$H_{gg^* \rightarrow gg}^{(1)} = \frac{N_c}{C_F} \frac{(\bar{s}^2 - \bar{t}\bar{u})^2}{\hat{t}\hat{t}\hat{u}\hat{u}\hat{s}\bar{s}} [\hat{t}\bar{t} + \hat{u}\bar{u}] , \quad (\text{A.6})$$

$$H_{gg^* \rightarrow gg}^{(2)} = \frac{N_c}{C_F} \frac{(\bar{s}^2 - \bar{t}\bar{u})^2}{\hat{t}\hat{t}\hat{u}\hat{u}\hat{s}\bar{s}} [\hat{s}\bar{s} - \hat{t}\bar{t} - \hat{u}\bar{u}] , \quad (\text{A.7})$$

$$H_{gg^* \rightarrow gg}^{(6)} = -\frac{N_c^2}{2} H_{gg^* \rightarrow gg}^{(3)} = N_c^2 H_{gg^* \rightarrow gg}^{(4)} = N_c^2 H_{gg^* \rightarrow gg}^{(5)} = \frac{N_c}{C_F} \frac{(\bar{s}^2 - \bar{t}\bar{u})^2}{\hat{t}\hat{t}\hat{u}\bar{u}} . \quad (\text{A.8})$$

The on-shell limit is again manifest, with the above equations reducing to Eqs. (4.36), (4.37) and (4.38) as  $|k_t| \rightarrow 0$ .

$gg^* \rightarrow q\bar{q}$	$D_i$
(1)	$\frac{1}{N_c} \frac{(\bar{s} + \bar{u})(2\bar{s}\bar{u} + \bar{s}^2 + 2\bar{u}^2)}{2\hat{t}\bar{s}(\hat{s} + \hat{t} + \hat{u})}$
(2)	$-\frac{1}{N_c} \frac{\bar{u}(2\bar{s}\bar{u} + \bar{s}^2 + 2\bar{u}^2)}{2\hat{u}\bar{s}(\hat{s} + \hat{t} + \hat{u})}$
(3)	$-\frac{1}{N_c^2 C_F} \frac{(2\bar{s}\bar{u} + \bar{s}^2 + 2\bar{u}^2)(\bar{s}(\hat{s} + \hat{t}) + \bar{u}(\hat{t} - \hat{u}))}{8\hat{t}\hat{u}\bar{s}(\hat{s} + \hat{t} + \hat{u})}$
(4)	$-\frac{1}{C_F} \frac{2\bar{s}\bar{u} + \bar{s}^2 + 2\bar{u}^2}{2\hat{s}(\hat{s} + \hat{t} + \hat{u})}$
(5)	$-\frac{1}{C_F} \frac{(2\bar{s}\bar{u} + \bar{s}^2 + 2\bar{u}^2)(\bar{s}(\hat{s} - \hat{t}) - \bar{u}(\hat{t} + \hat{u}))}{8\hat{s}\hat{t}\bar{s}(\hat{s} + \hat{t} + \hat{u})}$
(6)	$-\frac{1}{C_F} \frac{(2\bar{s}\bar{u} + \bar{s}^2 + 2\bar{u}^2)(\bar{s}(\hat{s} + \hat{t}) + \bar{u}(\hat{t} + \hat{u}))}{8\hat{s}\hat{u}\bar{s}(\hat{s} + \hat{t} + \hat{u})}$

Table 9: Expressions for the  $gg^* \rightarrow q\bar{q}$  subprocess with off-shell incoming gluon corresponding to diagrams (1)-(6) of Fig. 4 in gauge described in Section 5.

$gg^* \rightarrow gg$	$D_i$
(1)	$\frac{2N_c}{C_F} \frac{(\bar{t}\bar{u} + \bar{t}^2 + \bar{u}^2)^2}{\hat{t}\bar{u}(\bar{t} + \bar{u})(\hat{s} + \hat{t} + \hat{u})}$
(2)	$\frac{2N_c}{C_F} \frac{(\bar{t}\bar{u} + \bar{t}^2 + \bar{u}^2)^2}{\hat{u}\bar{t}(\bar{t} + \bar{u})(\hat{s} + \hat{t} + \hat{u})}$
(3)	$\frac{N_c}{2C_F} \frac{(\bar{t}\bar{u} + \bar{t}^2 + \bar{u}^2)^2(\bar{t}(\hat{s} + \hat{t}) + \bar{u}(\hat{s} + \hat{u}))}{\hat{t}\hat{u}\bar{t}\bar{u}(\bar{t} + \bar{u})(\hat{s} + \hat{t} + \hat{u})}$
(4)	$-\frac{2N_c}{C_F} \frac{(\bar{t}\bar{u} + \bar{t}^2 + \bar{u}^2)^2}{\hat{s}\bar{t}\bar{u}(\hat{s} + \hat{t} + \hat{u})}$
(5)	$-\frac{N_c}{2C_F} \frac{(\bar{t}\bar{u} + \bar{t}^2 + \bar{u}^2)^2(\bar{t}(\hat{s} - \hat{t}) + \bar{u}(\hat{s} + \hat{u}))}{\hat{s}\hat{t}\bar{t}\bar{u}(\bar{t} + \bar{u})(\hat{s} + \hat{t} + \hat{u})}$
(6)	$-\frac{N_c}{2C_F} \frac{(\bar{t}\bar{u} + \bar{t}^2 + \bar{u}^2)^2(\bar{t}(\hat{s} + \hat{t}) + \bar{u}(\hat{s} - \hat{u}))}{\hat{s}\hat{u}\bar{t}\bar{u}(\bar{t} + \bar{u})(\hat{s} + \hat{t} + \hat{u})}$

Table 10: Expressions for the  $gg^* \rightarrow gg$  subprocess with off-shell incoming gluon in gauge described in Section 5. The numbering (1)-(6) corresponds to the color structures as defined in Eq. (4.43) and each expression contains contributions from diagrams with both 3- and 4-gluon vertices.

## References

- [1] L. V. Gribov, E. M. Levin and M. G. Ryskin, Phys. Rept. **100** (1983) 1.
- [2] F. Gelis, E. Iancu, J. Jalilian-Marian and R. Venugopalan, Ann. Rev. Nucl. Part. Sci. **60** (2010) 463.
- [3] J. L. Albacete and C. Marquet, Prog. Part. Nucl. Phys. **76** (2014) 1.
- [4] J. L. Albacete and C. Marquet, Phys. Rev. Lett. **105** (2010) 162301.
- [5] A. Stasto, B. -W. Xiao and F. Yuan, Phys. Lett. B **716** (2012) 430.
- [6] T. Lappi and H. Mantysaari, Nucl. Phys. A **908** (2013) 51.
- [7] C. Marquet, Nucl. Phys. A **796** (2007) 41.
- [8] A. Adare *et al.* [PHENIX Collaboration], Phys. Rev. Lett. **107** (2011) 172301.
- [9] E. Braidot [STAR Collaboration], arXiv:1005.2378 [hep-ph].
- [10] S. Catani, M. Ciafaloni and F. Hautmann, Nucl. Phys. B **366** (1991) 135.
- [11] M. Deak, F. Hautmann, H. Jung and K. Kutak, JHEP **0909** (2009) 121.
- [12] C. J. Bomhof, P. J. Mulders and F. Pijlman, Eur. Phys. J. C **47** (2006) 147.
- [13] F. Dominguez, C. Marquet, B. -W. Xiao and F. Yuan, Phys. Rev. D **83** (2011) 105005.
- [14] F. Dominguez, B. -W. Xiao and F. Yuan, Phys. Rev. Lett. **106** (2011) 022301.
- [15] K. Kutak and S. Sapeta, Phys. Rev. D **86** (2012) 094043.
- [16] A. van Hameren, P. Kotko, K. Kutak, C. Marquet and S. Sapeta, Phys. Rev. D **89** (2014) 094014.
- [17] A. van Hameren, P. Kotko, K. Kutak and S. Sapeta, Phys. Lett. B **737** (2014) 335.
- [18] A. van Hameren, P. Kotko and K. Kutak, Phys. Rev. D **88** (2013) 9, 094001 [Erratum-ibid. D **90** (2014) 3, 039901].
- [19] D. Boer and P. J. Mulders, Nucl. Phys. B **569** (2000) 505.
- [20] A. V. Belitsky, X. Ji and F. Yuan, Nucl. Phys. B **656** (2003) 165.
- [21] D. Boer, P. J. Mulders and F. Pijlman, Nucl. Phys. B **667** (2003) 201.
- [22] J. Collins and J. W. Qiu, Phys. Rev. D **75** (2007) 114014.
- [23] W. Vogelsang and F. Yuan, Phys. Rev. D **76** (2007) 094013.
- [24] T. C. Rogers and P. J. Mulders, Phys. Rev. D **81** (2010) 094006.
- [25] B. W. Xiao and F. Yuan, Phys. Rev. Lett. **105** (2010) 062001.
- [26] M. L. Mangano and S. J. Parke, Phys. Rept. **200** (1991) 301.
- [27] A. H. Mueller, B. -W. Xiao and F. Yuan, Phys. Rev. Lett. **110** (2013) 082301.

- [28] A. H. Mueller, B. -W. Xiao and F. Yuan, Phys. Rev. D **88** (2013) 114010.
- [29] M. Ciafaloni, Nucl. Phys. B **296** (1988) 49.
- [30] S. Catani, F. Fiorani and G. Marchesini, Nucl. Phys. B **336** (1990) 18.
- [31] S. Catani, F. Fiorani and G. Marchesini, Phys. Lett. B **234** (1990) 339.
- [32] E. Iancu and J. Laidet, Nucl. Phys. A **916** (2013) 48.
- [33] K. Kutak, Phys. Rev. D **91** (2015) 3, 034021.
- [34] A. van Hameren, P. Kotko and K. Kutak, JHEP **1212** (2012) 029.
- [35] A. van Hameren, P. Kotko and K. Kutak, JHEP **1301** (2013) 078.
- [36] L. N. Lipatov, Sov. J. Nucl. Phys. **23** (1976) 338.
- [37] E. A. Kuraev, L. N. Lipatov and V. S. Fadin, Sov. Phys. JETP **44** (1976) 443 [Erratum-ibid. **45** (1977) 199].
- [38] I. I. Balitsky and L. N. Lipatov, Sov. J. Nucl. Phys. **28** (1978) 822.
- [39] J. Kwiecinski, A. D. Martin and A. M. Stasto, Phys. Rev. D **56** (1997) 3991.
- [40] I. Balitsky, Nucl. Phys. B **463** (1996) 99.
- [41] Y. V. Kovchegov, Phys. Rev. D **60** (1999) 034008.
- [42] K. Kutak and J. Kwiecinski, Eur. Phys. J. C **29** (2003) 521.
- [43] K. Kutak and A. M. Stasto, Eur. Phys. J. C **41** (2005) 343.
- [44] E. Akcakaya, A. Schfer and J. Zhou, Phys. Rev. D **87** (2013) 5, 054010.
- [45] L. N. Lipatov, Nucl. Phys. B **452** (1995) 369.
- [46] E. N. Antonov, L. N. Lipatov, E. A. Kuraev and I. O. Cherednikov, Nucl. Phys. B **721** (2005) 111.
- [47] P. Kotko, JHEP **1407** (2014) 128.
- [48] A. van Hameren, JHEP **1407** (2014) 138.
- [49] L. J. Dixon, arXiv:1310.5353 [hep-ph].
- [50] V. Del Duca, L. J. Dixon and F. Maltoni, Nucl. Phys. B **571** (2000) 51.
- [51] J. C. Collins, D. E. Soper and G. F. Sterman, Nucl. Phys. B **250** (1985) 199.
- [52] M. A. Kimber, A. D. Martin and M. G. Ryskin, Eur. Phys. J. C **12** (2000) 655.
- [53] M. A. Kimber, A. D. Martin and M. G. Ryskin, Phys. Rev. D **63** (2001) 114027.
- [54] J. Collins and T. Rogers, Phys. Rev. D **91** (2015) 7, 074020.
- [55] K. Kutak, K. Golec-Biernat, S. Jadach and M. Skrzypek, JHEP **1202** (2012) 117.
- [56] K. Kutak, JHEP **1212** (2012) 033.

- [57] X. d. Ji, J. p. Ma and F. Yuan, Phys. Rev. D **71** (2005) 034005.
- [58] F. Dominguez, A. H. Mueller, S. Munier and B. W. Xiao, Phys. Lett. B **705** (2011) 106.
- [59] V. S. Fadin, R. Fiore, M. G. Kozlov and A. V. Reznichenko, Phys. Lett. B **639** (2006) 74.